



Scanning tunneling microscopy

Paul K. Hansma and Jerry Tersoff

Citation: *J. Appl. Phys.* **61**, R1 (1987); doi: 10.1063/1.338189

View online: <http://dx.doi.org/10.1063/1.338189>

View Table of Contents: <http://jap.aip.org/resource/1/JAPIAU/v61/i2>

Published by the American Institute of Physics.

Related Articles

A compact sub-Kelvin ultrahigh vacuum scanning tunneling microscope with high energy resolution and high stability

Rev. Sci. Instrum. **82**, 103702 (2011)

Compact device for cleaning scanner-mounted scanning tunneling microscope tips using electron bombardment

Rev. Sci. Instrum. **82**, 083701 (2011)

Fabrication of silver tips for scanning tunneling microscope induced luminescence

Rev. Sci. Instrum. **82**, 083101 (2011)

Scanning tunneling spectroscopy under large current flow through the sample

Rev. Sci. Instrum. **82**, 073710 (2011)

Haptic-STM: A human-in-the-loop interface to a scanning tunneling microscope

Rev. Sci. Instrum. **82**, 073704 (2011)

Additional information on J. Appl. Phys.

Journal Homepage: <http://jap.aip.org/>

Journal Information: http://jap.aip.org/about/about_the_journal

Top downloads: http://jap.aip.org/features/most_downloaded

Information for Authors: <http://jap.aip.org/authors>

ADVERTISEMENT



AIP Advances

Submit Now

Explore AIP's new
open-access journal

- Article-level metrics now available
- Join the conversation! Rate & comment on articles

Scanning tunneling microscopy

Paul K. Hansma

Department of Physics, University of California, Santa Barbara, California 93106

Jerry Tersoff

IBM T. J. Watson Research Center, Yorktown Heights, New York 10598

(Received 23 June 1986; accepted for publication 9 September 1986)

A scanning tunneling microscope (STM) can provide atomic-resolution images of samples in ultra-high vacuum, moderate vacuum, gases including air at atmospheric pressure, and liquids including oil, water, liquid nitrogen, and even conductive solutions. This review contains images of single-crystal metals, metal films, both elemental and compound semiconductors, superconductors, layered materials, adsorbed atoms, and even DNA. A discussion of results on lithography leads into speculations on a bright future in which STMs may not only observe, but also manipulate surfaces, right down to the atomic level.

I. INTRODUCTION

Scanning tunneling microscopy¹⁻³ reveals three-dimensional pictures of surfaces—even individual atoms. The left-hand column of Fig. 1 shows the basic “constant current” mode of operation.¹⁻³ A tip is brought close enough to the surface that, at a convenient operating voltage (2 mV–2 V), the tunneling current is measurable. The tip is scanned over a surface while the current I , between it and the surface, is sensed. A feedback network changes the height of the tip z to keep the current constant. Since the current varies exponentially with the gap between the tip and the surface, this keeps the gap nearly constant. An image consists of a map $z(x,y)$ of tip height z versus lateral position x,y . The simplest scheme for plotting the image is shown in the graph below the schematic view. The height z is plotted versus the scan position x . An image consists of multiple scans displaced laterally from each other in the y direction. The pseudo-three-dimensional appearance results from plotting a weighted combination of z and y vs x .

Alternatively, in the constant height mode⁴ a tip can be scanned across a surface at nearly constant height and constant voltage while the current is monitored, as shown in the right-hand column of Fig. 1. In this case the feedback network responds only rapidly enough to keep the average current constant. As shown in the graph below the schematic view, the rapid variations in current due to the tip passing over surface features such as atoms, are plotted versus scan position. Again, an image consists of multiple scans displaced laterally from each other in the y direction. In this case a weighted sum of I and y is plotted versus x .

In the constant height mode it is also possible to scan the tip across a surface at nearly constant height and constant current while the voltage is monitored. In this case the feedback network responds only rapidly enough to keep the average voltage constant. The rapid variations in voltage due to the tip passing over surface features such as atoms, are plotted versus scan position.

Each mode has its own advantages. The basic constant-current mode was first historically and has been used for almost all the images in this review. It reduces to a classical topograph in the limit of dimensions $\gtrsim 10 \text{ \AA}$. It can be used

to track surfaces which are not atomically flat. On the other hand, the constant height mode allows for much faster imaging of atomically flat surfaces since only the electronics—not the z translator—must respond to the atoms passing under the tip. The fastest scan rate in currently published articles is $\sim 10 \text{ Hz}$ for the basic mode, but 1 kHz for the constant height mode. Fast imaging is important in both modes since it may enable researchers to study processes in real time as well as reducing data collection time. Fast imaging also minimizes image distortion due to piezoelectric creep and thermal drift.

For both modes of operation the images can be plotted

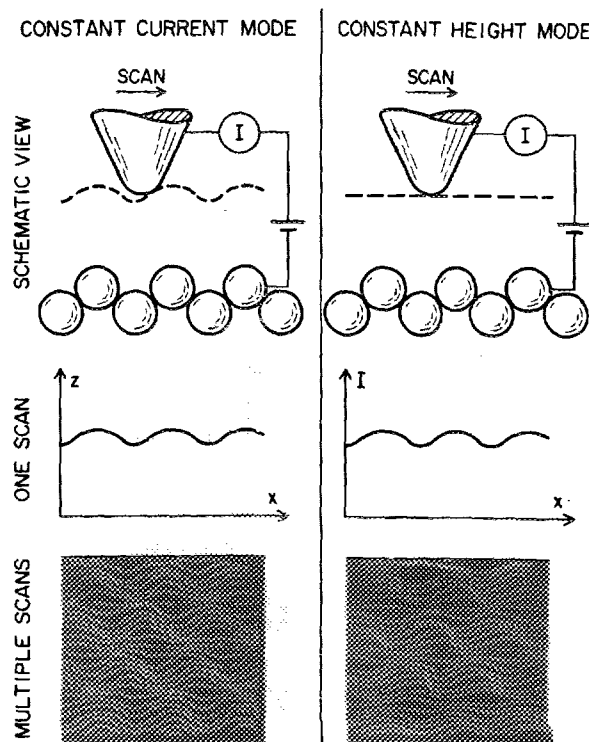


FIG. 1. Scanning tunneling microscopes can be operated in either the constant current mode or the constant height mode. The images are of graphite in air taken by R. Sonnenfeld.

in various other ways. For example, the darkness at each point (x,y) in the image can be determined by the height z , or current I , or voltage V , producing a grey-scale image as shown in Fig. 2.⁵ Similarly the color at each point (x,y) in the image can be determined by z , I , or V producing a false color image, beautiful to behold, but not publishable in most journals. Line images can be enhanced by various computer assisted techniques such as hidden line suppression, cross hatching between lines, and rotation. As shown in Fig. 3, rotation can sometimes make surface features easier to see.⁶

The rest of this review begins with the invention of scanning tunneling microscopy, and continues with a section on theory that emphasizes the aspects that relate directly to the interpretation of experimental images. Next, the section on experimental methods tells the basic physics, technology and tricks involved in building a tunneling microscope. Then the experimental results section displays representative work of twelve groups and discusses the work of more. This section is divided into subsections on metals, semiconductors, superconductors, and low-temperature spectroscopy, layered materials, adsorbed materials and biological materials, lithography, and speculations on the future. Finally, after the summary and acknowledgments there is an appendix on vibration isolation.

II. DISCOVERY

The recent rapid growth in scanning tunneling microscopy began with the pioneering work of G. Binnig, H. Rohrer, Ch. Gerber, E. Weibel, and their collaborators at IBM Zürich Laboratories. Figure 4 shows a schematic view of one of their designs⁷ together with magnified views of the tip and sample. It was fascinating enough when they reported obtaining first tunneling⁸ and then images,^{1,2} but real excitement started with their observation of atomic scale features on a silicon surface,³ reconstructed metal surfaces,^{8,9} and chemisorbed molecules.¹⁰ These observations and others that they have made will be discussed in Sec. V.

The development of tunneling microscopy was anticipated by a similar device, the topografiner,^{11,12} developed by

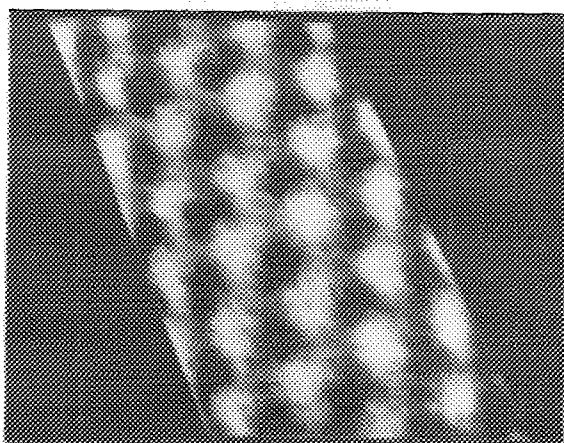


FIG. 2. Grey-scale images of a surface are especially helpful in determining the lattice of periodic features. Figure from Binnig and Smith (see Ref. 5).

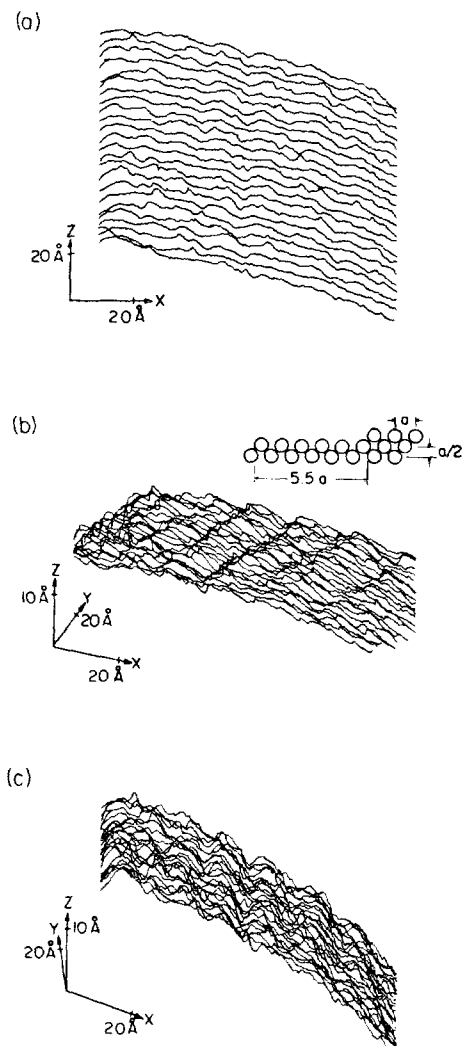


FIG. 3. Image manipulation such as the rotations shown here can help reveal features such as parallel rows. Figures from Abraham (see Ref. 6).

Russell Young, Clayton Teague, and collaborators at the National Bureau of Standards ten years before the development of the scanning tunneling microscope. Figure 5 shows line images of a diffraction grating taken with the "topografiner."

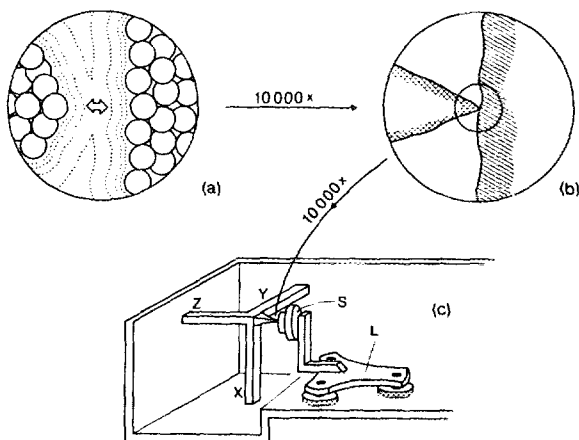


FIG. 4. A schematic view of the heart of one of the IBM Zürich designs. Figure from Binnig and Rohrer (see Ref. 7).

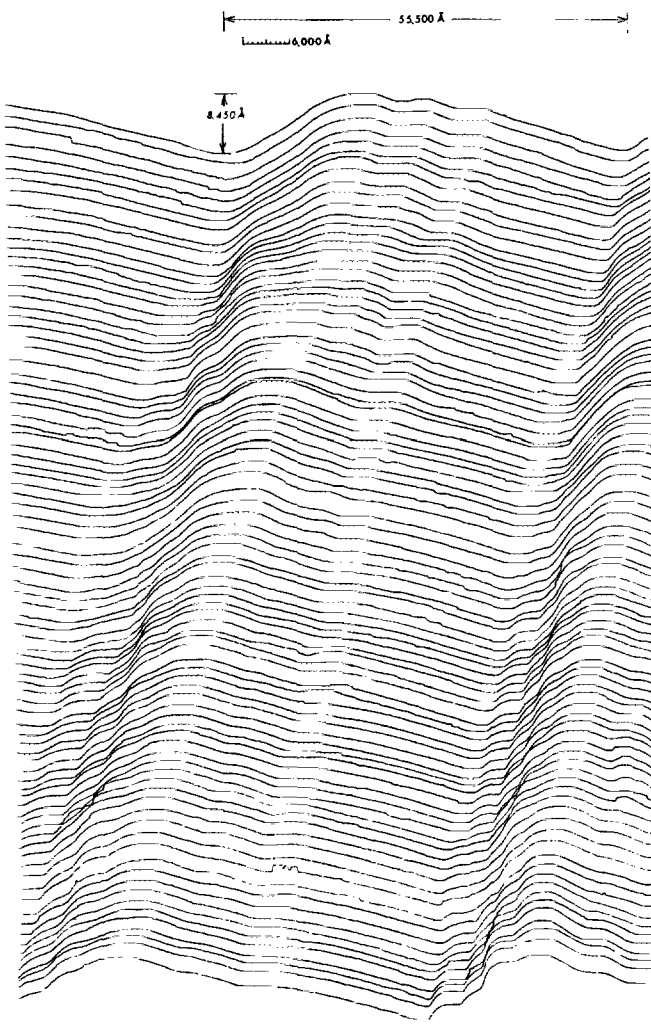


FIG. 5. Topografiner image of a 180-line/mm diffraction grating replica. Figure from Young, Ward, and Scire (see Ref. 12).

Figure 6 shows previously unpublished work of theirs that may anticipate further development in tunneling microscopy. In this image the output of a channeltron electron multiplier pointed at the surface is plotted in a grey scale image as a function of the position of the tip above the sur-

face. In the future, researchers may find it useful to plot the output of this and other devices monitoring the surface while the surface is being scanned with the tip. For example, it might be fruitful to plot the light output from a rough silver surface being scanned with a tip at relatively high bias voltage (> 2 V) to study the details of the electron-to-photon conversion efficiency at various topographic features.

III. THEORY

A. Introduction

One of the very appealing features of STM is that it gives images which appear to be simply direct topographs of the surface. This view, although somewhat naive, is quite adequate in many cases.¹ However, with the advent of "atomic resolution" imaging,³ it became apparent that a more microscopic understanding of STM was required. Here we survey theoretical work in STM, emphasizing those aspects of the theory which relate directly to the interpretation of experimental images.

Early analyses¹ of the tunneling current and STM image were based on analogy with the one-dimensional tunneling problem. There it is well known that the tunneling current (at low voltage and temperature) behaves as

$$I \propto \exp(-2\kappa d), \quad (1)$$

where I is the current, d is the distance between electrodes, and κ is the decay constant for the wave functions in the barrier. In this case of vacuum tunneling, κ is related to the effective local work function ϕ by

$$\kappa = \hbar^{-1} \sqrt{2m\phi}, \quad (2)$$

where m is the electron mass.

For a typical work function of 4 eV, $\kappa = 1.0 \text{ \AA}^{-1}$, and the current decreases by an order of magnitude when the gap d is increased by only 1 Å. If the current is kept constant to within, e.g., 2%, then the gap d remains constant to within 0.01 Å. This fact is the basis for interpreting the image as simply a contour of constant height above the surface.

Unfortunately, this simple picture breaks down just when STM becomes really interesting. When an atomically sharp tip is scanned across a plane of atoms in constant-current imaging mode, yielding an image with subangstrom

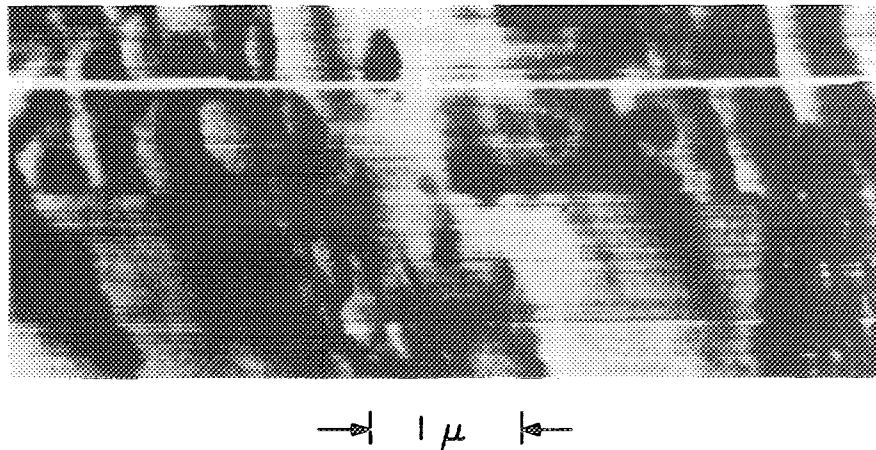


FIG. 6. Grey-scale image of a Channeltron detector output vs position of the topografiner tip. Figure from R. Young (previously unpublished).

corrugations, it is not clear exactly what distance might play the role of d in (1). Moreover, since tunneling involves states at the Fermi level, which themselves may have a complex spatial structure, we must expect that the electronic structure of the surface and tip may enter in a complex way. Many researchers have therefore recently considered the full three-dimensional tunneling problem as it relates to STM.¹³⁻²⁰

B. Tunneling current

At the surface-tip separations of interest in STM, of order 4 Å or more, the surface-tip interaction is extremely weak. It is natural then to calculate the tunneling current in first-order perturbation theory, which is essentially exact in this case. At low temperatures, this current is just

$$I = \frac{2\pi e}{\hbar} \sum_{\mu\nu} f(E_\mu) [1 - f(E_\nu + eV)] |M_{\mu\nu}|^2 \delta(E_\mu - E_\nu), \quad (3)$$

where $M_{\mu\nu}$ is the tunneling matrix element, $f(E)$ is the Fermi function, V is the voltage across the barrier, and E_μ is the energy of the state μ , where μ and ν run over all the states of the tip and surface, respectively.

Bardeen showed²¹ that the tunneling matrix element $M_{\mu\nu}$ could be written in a particularly convenient form, which requires knowledge only of the wave functions of the two electrodes separately. Specifically,

$$M_{\mu\nu} = \frac{\hbar^2}{2m} \int d\mathbf{S} \cdot (\Psi_\mu^* \nabla \Psi_\nu - \Psi_\nu \nabla \Psi_\mu^*), \quad (4)$$

where Ψ_ν is the wave function, and the integral is over any plane in the barrier region. The quantity in parentheses is just the current operator. In principle, (3) and (4) are all that is needed to calculate the current, and hence the STM image.

This result has been exploited by many groups to study the STM tunneling current.¹³⁻¹⁸ Most recently, Lang showed¹⁷ that (3) and (4) could be generalized to obtain an explicit formula for the current density $j(r)$, and he reported¹⁸ the first calculations in which both the surface and tip consisted of real atoms instead of a model potential well. Figure 7 shows the calculated¹⁸ current density distribution in the vacuum barrier between a surface and tip, each consisting of a single atom adsorbed on a jellium surface.

In addition, a few groups^{19,20} have studied the tunneling current by calculating the transmission coefficient for electrons incident on a corrugated barrier. However, this approach has significant disadvantages,¹⁶ and it has not been actively pursued since those early studies.

C. Interpretation of images

The theory of tunneling makes no distinction between surface and tip. However, in STM, this distinction is crucial. Ideally, one would like to relate the STM image directly to a property of the surface, whereas in any exact analysis the current involves a complicated convolution of the electronic spectra of surface and tip.¹³⁻¹⁶

Tersoff and Hamann observed¹⁴ that the tip properties can be taken out of the problem by considering a particular model for the tip, motivated as follows. The ideal scanning

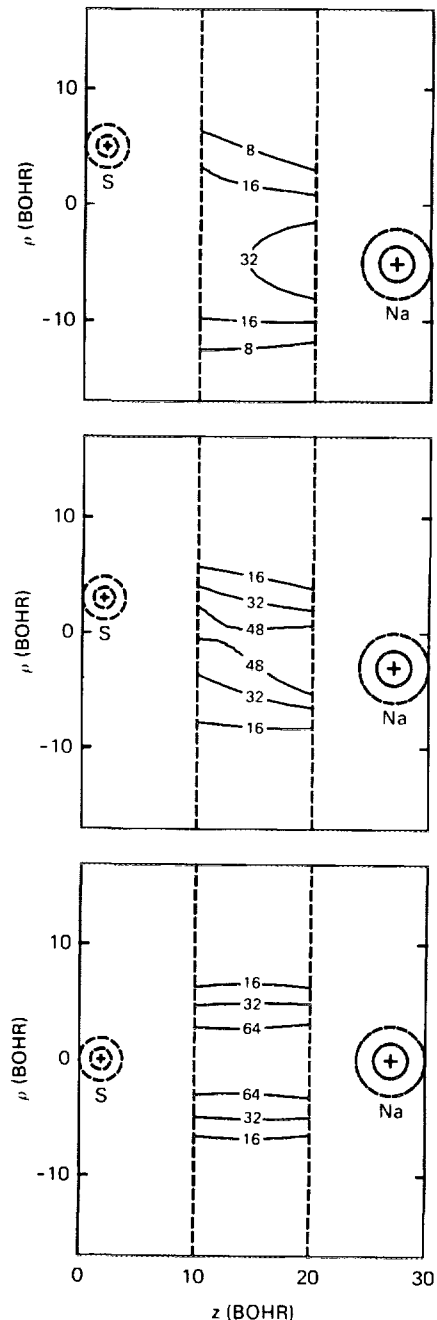


FIG. 7. Contour map of current density (relative to background current between jellium electrodes) j_z/j_0 for S adatom on the left electrode and Na adatom on the right electrode, for three values of the lateral separation (10, 6, and 0 Bohr), in the plane normal to the surfaces that includes both nuclei. Figure from Lang (see Ref. 18).

tunneling microscope would have the greatest possible resolution, and would measure an intrinsic property of the unperturbed surface, rather than a property of the joint surface-tip system. These goals would be best achieved by a tip whose potential and wave functions were arbitrarily localized. In that case, in the limit of small voltage, the tunneling conductance is¹⁴

$$\sigma \propto \rho(\mathbf{r}_t, E_F), \quad (5)$$

where \mathbf{r}_t is the tip position, E_F is the Fermi energy, and

$$\rho(\mathbf{r}, E) \equiv \sum_\nu |\Psi_\nu(\mathbf{r})|^2 \delta(E_\nu - E) \quad (6)$$

is the surface local density of states (LDOS) at point \mathbf{r} and energy E . (We speak of conductance rather than current since the former becomes independent of voltage in the limit of small voltage.)

In this simple limit, then, the STM image has a straightforward interpretation. The current is proportional to the surface LDOS at E_F at the tip position, so the tip path maps out a contour of constant Fermi-level LDOS of the bare surface. Tersoff and Hamann^{13,14} showed that this result could be extended to a tip of arbitrary size, as long as the tip wave functions at E_F could be adequately approximated by an s -wave wave function, and \mathbf{r}_t is taken as the center of curvature of the tip wave function. They also gave an explicit formula for the proportionality constant. Moreover, including higher l -wave components in the wave function was shown to give only minor quantitative modifications for reasonably small l . Therefore, (5) is almost certainly adequate whenever the tip is effectively a single atom, and is probably fine even for a small cluster of atoms, as long as the effective center is suitably chosen.

In fact, the accuracy of (5) for an atomically sharp tip has recently been directly confirmed by Lang,¹⁸ who performed essentially exact calculations using the real wavefunctions of the surface and tip shown in Fig. 7. Figures 8 and 9 compare the images obtained from the full calculation (solid line) with the almost identical result of (5) (dot-dashed line).

By relating the image to a property of the surface alone, it becomes possible to calculate STM images for real surfaces. The required calculation (6) is very similar to the calculation of charge density (although more demanding numerically), and so standard methods can be applied. To date, such calculations have been reported for only a very few surfaces.^{13,14,22}

As an example, the results for Au(110) are shown in Fig. 10. If an effective tip radius of 9 Å is assumed, then the tip center of curvature is expected to follow the dashed contours. With this one assumption, the corrugation amplitudes calculated for both surfaces were in quantitative agreement with experiment,⁹ as was the vacuum gap distance.

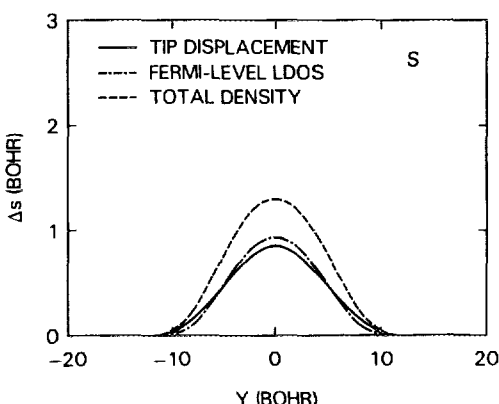


FIG. 8. Comparison of calculated tip displacement curve, for model illustrated in Fig. 7, with contours of constant Fermi-level local density of states, and constant total charge density. Figure from Lang (see Ref. 18).

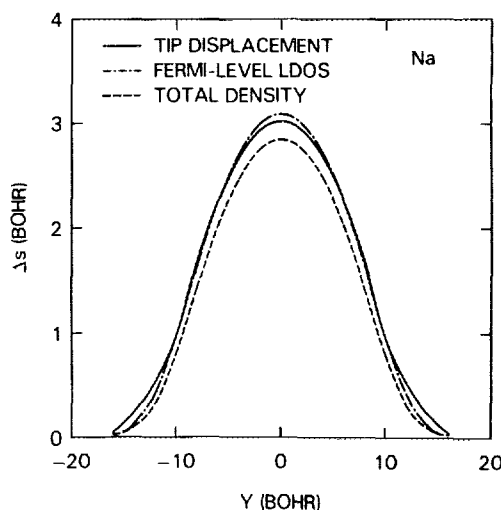


FIG. 9. Same as Fig. 8, for case where both adatoms are Na. Figure from Lang (see Ref. 18).

D. Resolution

By examining the properties of $\rho(\mathbf{r}, E)$, it is possible to derive some general results concerning the STM image. In particular, one can estimate the resolution, as has been done by Tersoff and Hamann,^{13,14} and by Stoll.²³

Some care is required in discussing STM resolution. Normally resolution is defined in terms of an ideal image $I_0(x)$, an instrumental resolution function $F(x)$, and a resulting experimental image which is a convolution of the two:

$$I(x) = \int F(y) I_0(x - y) dy. \quad (7)$$

Thus to define the resolution requires first defining the ideal image I_0 . If F were known exactly, then in the absence of noise one could deconvolute the experimental image, and no information would be lost even with a poor nominal resolution, i.e., a broad function F .

One could, of course, choose the contour of constant $\rho(\mathbf{r}, E_F)$ which the tip follows as I_0 . In that case the STM image [within the level of approximation of (5)] represents I_0 exactly, and so the resolution is perfect. However, the STM image becomes less corrugated, and loses its detailed features, as the tunneling distance (or tip size) is increased. It seems attractive, therefore, to try defining I_0 to be some property in the plane of the surface, and then relate the image to a convolution of I_0 with an instrumental resolution function.^{13,14,23}

While such a deconvolution is not possible in general for a nonlinear imaging process, in the limit of small corrugation the problem can be linearized, and so a resolution function can be defined. One then finds^{13,14,23} that the resolution may be characterized by a function F whose rms width W is typically

$$W \approx (z/2\kappa)^{1/2} \quad (8)$$

under certain reasonable assumptions. Here z is the sum of the tip radius and the vacuum gap distance. For example, with a single atom tip one might find z as small as 5 Å, in which case $W \approx 1.6$ Å.

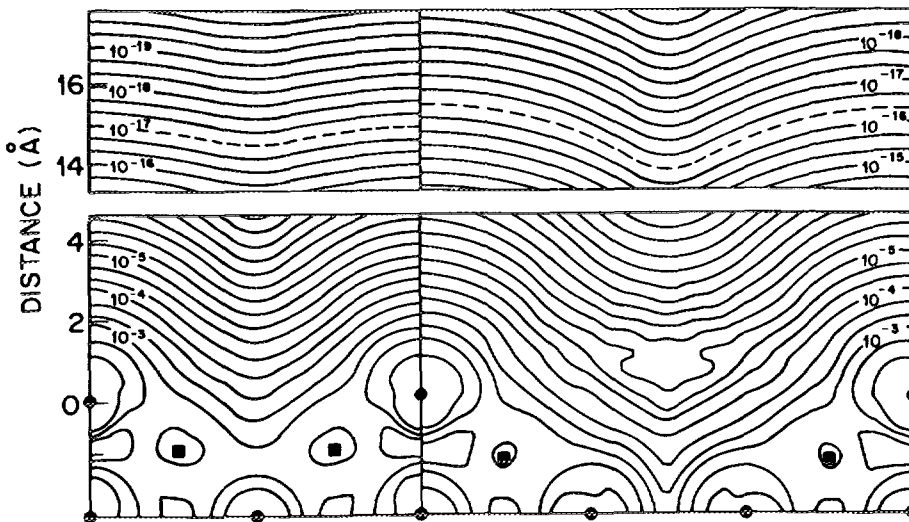


FIG. 10. Calculated (ρ, E_F) for Au(110) 2×1 (left) and 3×1 (right) surfaces. Positions of nuclei are shown by solid circles (in plane) and squares (out of plane). Peculiar structure around contour 10^{-5} of 3×1 is due to limitations of the planewave part of the basis in describing the exponential decay inside the deep troughs. Figure from Tersoff and Hamann (see Ref. 13).

Often one is not interested in the nominal resolution, but rather in the ability of the instrument to separate two peaks, or to detect the atomic corrugation of a relatively close-packed surface. This ability depends on both the resolution and the noise level. We may choose as a criterion of sensitivity that the signal-to-noise ratio be at least 1:1. Then for a surface with lattice constant a , if the noise with Fourier component $G = 2\pi/a$ has an amplitude n_G , the signal [i.e., the corrugation of $\rho(r, E_F)$] must have a least equal amplitude to be reliably measured. In the small-corrugation limit valid far from the surface, the corrugation is roughly¹⁴

$$\Delta \approx 2\kappa^{-1} \exp(-zG^2/4\kappa) \\ \approx 2\kappa^{-1} \exp(-G^2 W^2/2). \quad (9)$$

The criterion $\Delta \geq n_G$ may then be rewritten

$$a \geq [2\pi^2/\ln(2/\kappa n_G)]^{1/2} W \\ \approx 4[\ln(2 \text{ \AA}/n_G)]^{-1/2} W, \quad (10)$$

where a is the closest that equivalent atoms may be and still satisfy the signal-to-noise criterion.

Note that a is proportional to W , but also depends somewhat upon the noise level. For example, with a noise amplitude of 0.1 \AA , one finds that only atoms separated by at least 4 \AA or so can be accurately resolved. This is consistent with the best resolution normally obtained in STM of metal surfaces. Note that this estimate is relatively insensitive to the precise noise level assumed in (10), and even to the tip-surface distance in (8), as long as physically reasonable values are used.

While the assumptions underlying the above results (8)–(10) are reasonably general, they may still fail drastically in special cases. For example, in the case of graphite, it was recently shown²⁴ that the resolution and sensitivity become essentially infinite in the nominal limit (5), when (8)–(10) are rederived taking account of the fact that the projection of the Fermi surface onto the surface Brillouin zone is concentrated very near the corner of the Brillouin zone. As a result, the unit cells may be clearly distinguished in the experimental image, even though they are only 2 \AA apart. Some related

enhancement in the resolution may also occur for semiconductors, if the tunneling is to surface states near the Brillouin zone edge.

E. Image simulation for data analysis

So far we have emphasized that the simplicity of the result (5) for the STM image permits direct calculation of images for real surfaces. However, this is only practical at present for rather simple surfaces with small unit cells. For large-periodicity reconstructions, such as the Si(111) 7×7 surface, and especially for disordered surfaces, calculations of the surface electronic structure are simply not feasible.

In addition, for theoretical calculations to be truly useful in analyzing experimental data, it is necessary that one be able to calculate images for a variety of possible models for the surface, so as to see which if any are compatible with the experimental data. However, the calculations required for even a single fairly simple surface geometry may tax the limits of present computational capabilities,^{13,14} rendering such an analysis impractical.

In response to these problems, Tersoff and Hamann proposed¹⁴ a crude but extremely convenient scheme for calculating the STM image without any calculation of the electronic structure. They showed¹⁴ that, under certain reasonable assumptions, the real image would in many cases bear a strong similarity to the total charge density. This result was confirmed in calculations by Lang,¹⁸ especially in the case of metallic atoms, as shown in Fig. 9. (Even for a nonmetallic atom Lang found good qualitative agreement between the charge density contour and the full image, as in Fig. 8.) The most severe approximation in the simplified scheme is that the charge density was then modelled by a superposition of atomic charge densities.^{14,25}

This scheme is best suited to simple and noble metals, and was shown¹⁴ to describe the experimental results in the case of Au surfaces just as well as the full calculation. Such a simplistic approach may however be expected to fail drastically in some cases, in particular for chemically heterogeneous surfaces.²⁵ The scheme also fails when the states at E_F

are concentrated in a small part of the surface Brillouin zone, as frequently happens for quasi-two-dimensional materials, or for tunneling to surface states.²⁴

Nevertheless, the method was used with remarkable success by Tromp, Hamers, and Demuth²⁶ to interpret images of the Si(111) 7×7. This approach made it possible, for the first time, to unambiguously extract detailed structural information from the STM images of that surface. Those authors²⁶ collected a number of structural models which had been proposed as "consistent" with the STM images of Si(111) 7×7, and simulated the expected images using the method of Ref. 14. These were compared with experimental images taken under bias conditions chosen to minimize the effect of surface electronic structure. Only the adatom models bore a quantitative resemblance to the experimental images, and in particular the model proposed by Takayanagi gave almost perfect agreement with the simulated image throughout the unit cell.²⁶

This remarkable level of agreement is illustrated in Fig. 11, which compares the experimental image with the simulated images for various models. Of course, there is no reason in general to expect atom superposition to give such quantitative agreement with experiment, and for Si(111) 7×7 this agreement was found only under particular bias conditions. Nevertheless, it is hard to imagine that such agreement could occur for a model which did not correspond in its essentials to the actual surface structure.

F. Spatially resolved tunneling spectroscopy

As demonstrated by the work of Tromp, Hamers, and Demuth,²⁶ the use of STM as a tool for determining surface structure has already reached quite an advanced stage. A newer application of STM is spatially resolved surface tunneling spectroscopy. In this approach, one varies the tunneling voltage in order to obtain current-voltage spectra from specific points on the surface. Peaks in the derivatives of these spectra are interpreted as corresponding to energies of high LDOS, e.g., surface states or resonances. Alternatively, images (or voltage derivatives of images) may be taken at specific bias voltages to highlight the spatial distribution of

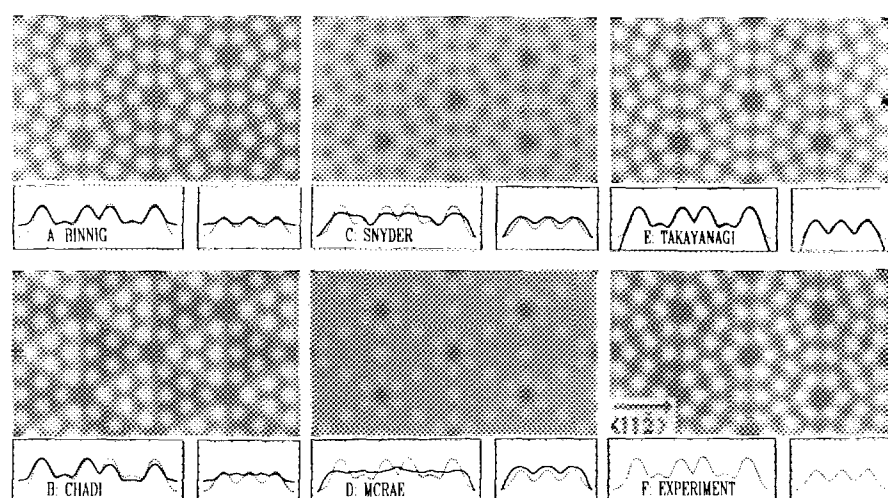


FIG. 11. Comparison between atom superposition simulation of STM images for various proposed structures of the Si(111) 7×7 surface, and experimental image (bottom right) taken at sample 2 V positive. Grey scale corresponds to 2 Å black to white, centered on mean height for each model. Line scans are between corner holes along long and short diagonals. Figure from Tromp, Hamers, and Demuth (see Ref. 26).

particular states. Only a few such investigations have so far been reported experimentally, using various modes (spectra at constant current or constant tip position, images at a given voltage at constant current, or constant height above the surface).^{27,28}

In principle, the tunneling at arbitrary voltage (below the field emission threshold) can be calculated from (3) and (4). The only theoretical calculations so far for STM spectroscopy were reported by Selloni *et al.*²² By assuming that the voltage dependence of the transmission coefficient through the barrier can be neglected relative to the voltage dependence of the density of states, and that the tip density of states is sufficiently featureless, they obtained the formula

$$\frac{dI}{dV} = \rho(\mathbf{r}, E_F + eV) T(V) \quad (11)$$

for the differential conductance, where $T(V)$ is the transmission coefficient of the barrier at voltage V .

Contour plots of surfaces of constant $\rho(\mathbf{r}, E_F + eV)$ were calculated²² for graphite at several voltages V , and these are shown in Fig. 12. The unexpectedly large corrugation at small voltage, and the strong voltage dependence of the corrugation, were subsequently confirmed experimentally.²⁹ Of course, the precise relationship between dI/dV and the spectra or images depends on the experiment mode used in taking the data.

IV. EXPERIMENTAL METHODS

A. x, y, and z translators

All published images so far have come from instruments that use piezoelectric elements as x , y , and z translators. These elements have been in the form of blocks, intricate shapes cut from blocks, rods, and bimorphs. A particularly elegant design using a single tube has recently been described by Binnig and Smith.³⁰

The primary design goal for the translators is to have them as rigid as possible for a given scan range. Specifically, the figures of merit are the resonant frequencies of the translator assembly in each orthogonal direction. These frequencies should definitely be above 1 kHz; frequencies above 30

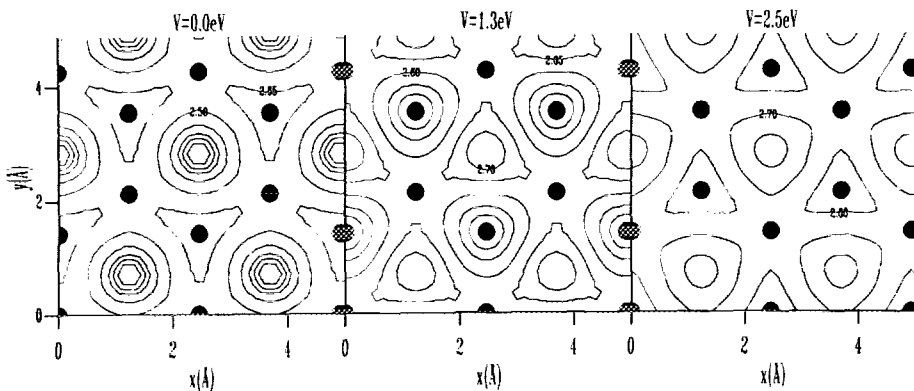


FIG. 12. Contour map of surface of constant $\rho(\rho, E_F + eV)$ for graphite, at several voltages corresponding to interesting features in the density of states. Figure from Selloni *et al.* (see Ref. 22).

kHz have been achieved; frequencies above 100 kHz are achievable.

It is important to have the resonant frequencies high not only because they determine the speed with which the microscope can be scanned, but also because they determine its rigidity against vibration.

B. Vibration Isolation

The first tunneling microscope used superconducting levitation for vibration isolation, the next generation used damped springs, air tables, and rubber mounts. Some recent IBM microscopes use compact stacks of stainless steel and Viton. In general the trend has been toward compactness and simplicity since it has become clear that increasing the rigidity of microscopes can be more conveniently achieved than perfecting a vibration isolation system. Nevertheless, it is true that the performance of a given microscope can be improved by improving the vibration isolation. It is therefore worth spending a little time, if you have not already, on the basis of vibration isolation as applied to tunneling microscopy. The Appendix has a very simple treatment. More advanced treatments can be found in mechanical engineering texts.

In the future compact, active vibration isolation systems may be developed and found to be desirable to enhance the performance of a microscope with given rigidity. Passive vibration isolation systems with good attenuation at typical building resonances (~ 20 Hz) must be large. Thus they are specially suited to microscopes that operate in air, gases or fluids because these microscopes usually don't have the space or vacuum compatibility problems encountered with ultra-high vacuum (UHV) instruments.

C. Coarse sample positioning

In the first modern tunneling microscopes the coarse sample positioning (to within the scan ranges of the x , y , and z translators) was done with a "Louse," a piezoelectric walker shown as "L" in Fig. 4. The Louse cannot only advance the sample toward the tip, but also move it laterally, and even back it away and rotate it to face other surface analytical equipment.

Some researchers have, however, sacrificed some of the freedom of motion provided by a Louse to obtain simpler

and smoother coarse sample positioning. For example, Demuth has developed an elegant mechanical system with one rotary feedthrough providing not only smooth, precise positioning when the tip is close to the sample but also a large range of motion (several cm) when it is further away from the sample.

Two generally useful techniques are (1) differential springs and (2) levers. For a differential spring mechanism a precise linear motion (often micrometer driven) deforms a weak spring with spring constant k_1 . This spring is connected to a sample support that flexes with a much larger spring constant k_2 to advance the sample toward the tip. For example, if the ratio of spring constants is $k_2/k_1 = 1000$, a 1-in. travel micrometer adjustable to 0.001 in. will give 25 μm of sample motion adjustable to 250 \AA .

Similarly, fine-pitched screws can drive one end of a lever that pivots near the sample. For example, a 80 thread per cm screw, driven by a rotary feedthrough with a 50-to-1 reduction gear, driving a lever with a 10-to-1 mechanical disadvantage over a range of 2 mm will give 200 μm of sample motion adjustable to roughly 7 \AA per degree motion of the rotary feedthrough.

D. Tip preparation

When tunneling microscopists got together in the past a big topic of conversation was the latest recipes for tip preparation. Almost all experiments to date have been done with tungsten wires either ground (on a grindstone!) or etched to a radius typically in the range 0.1–10 μm .

These sharpened wires sometimes produce atomic resolution images with no further treatment indicating that there was at least one atomically sharp tip projecting out from the (relatively dull) end. More generally, a recipe for *in situ* processing was used. Sample recipes are as follows.

(1) Withdraw the tip more than 1000 \AA from the sample. Apply a high enough voltage (of order several hundred volts) to get a field emission current of a few microamps, turn down the voltage as soon as any sudden jump in the current occurs (useful only in high vacuum).

(2) Apply an oscillating voltage at ≈ 1 kHz to the z piezo in addition to the feedback voltage. Increase the magnitude of the oscillating voltage until there is an abrupt change in the feedback voltage.

(3) Set up in a tunneling configuration with the tip scanning over the surface and just wait about 10 min to 1 h.

After the tip was formed by methods (1) or (2) it was prudent to move it laterally to a new region of the sample since these methods for tip forming could modify the surface directly under the tip.

More recently there is a growing consensus that an etched tip that appears sharp under a high-quality optical microscope (operated at $200\times$ or above) *will give atomic resolution almost every time* either immediately or after a wait as listed in method (3)—*if* it is not banged into the surface and thus flattened. “Appears sharp” means that no radius can be observed at the end with the optical microscope. This in turn means that the tip radius is $\leq 2000\text{ \AA}$.

Clearly, however, tip characterization and preparation is still an important area for future developmental work. At least two groups (H. Fink at IBM Zürich and Y. Kuk and P. J. Silverman at Bell Laboratories) are working with instruments to do tip characterization with field ion microscopy (FIM) and STM in the same vacuum system.

A beautiful film by Fink showing the reproducible creation of a tip terminated with a triad of atoms by the techniques of field ion microscopists was a highlight of a 1985 conference on STM in Oberlech, Austria.

E. Electronics

The electronics for STM is straightforward. Most of the pieces are commercially available. Basically, what is needed is (1) a source for the x and y raster voltages, (2) high-voltage amplifiers to drive the piezoelectric elements, (3) a voltage source and current sensing amplifier to establish and sense the tunneling current between the tip and the sample, (4) an error amplifier to amplify and (usually) integrate the difference between the tunneling current and some set-point current, and (5) a display device for the images. Many laboratories use a computer for (1) and (5). Other laboratories use function generators for (1) and a storage oscilloscope, chart recorder, or image recorder for (5).

The high-voltage amplifiers can be homebuilt but are available commercially (e.g., from Kepco). The voltage source and current sensing amplifier are available commercially. The voltage source is easy with no special requirements. The current sensing amplifier is easy for scan rates $\leq 10\text{ Hz}$ and more difficult for higher scan rates. Commercial current amplifiers (e.g., Keithly 427) have been used by several groups for scan rates $\leq 1\text{ Hz}$. Somewhat faster is a commercial low-noise amplifier (e.g., PAR 113) looking at the voltage across a $10^5\text{--}10^6\Omega$ resistor in series with the junctions. The fastest is a compact current-sensing amplifier very close to the junction to minimize capacitance. This can, however, be a problem in baked vacuum systems.

The one instrument that most researchers have had custom built (or built themselves) is the error amplifier. The main reason is that it turns out to be useful to have a logarithmic amplifier (e.g., Analog Devices AD 755P) to linearize the feedback loop since the tunneling current is exponentially dependent on distance. This desirable, but not essential, logarithmic amplifier is usually followed by the comparator for set point current and then an integrator. The integrator has infinite gain at dc so there will be no net, long-term difference between the operating current and the set point cur-

rent. The overall gain of the error amplifier is adjusted to be as high as possible without causing oscillations. Here again, the more rigid the microscope, the higher its resonant frequencies, and the higher the gain can be set. Typically it can be set for unity gain at a frequency of order 1 kHz. This adjustment should, however, be easily accessible and adjustable over a wide range since the optimal setting changes with tip condition and effective work function.

Sometimes a small additional increase in gain and hence speed of response can be obtained by putting a low pass filter with cutoff frequency above the unity gain point but below the resonant frequency. Further details on optimization of feedback systems are beyond the scope of this article.

A sometimes difficult decision is whether or not to computerize the apparatus, specifically, whether to use a computer to at least supply the x and y raster voltages and record the images (and perhaps also determine bias voltage and tunneling current, control tip advance, etc.). The advantages include flexibility, elegance, and image enhancement. For operation in UHV, where images are stable for minutes or even hours, the choice of most researchers has been to computerize.

For operation in air or liquids, where images can change in seconds, researchers have tended to use function generators and storage oscilloscopes or image enhancers. For example, Bryant, Smith, and Quate⁴ have used raster scan rates of over 1 kHz, and recorded over 10^4 images per hour on a VCR via an image enhancer (Arlunya TF5111). The images can be played back later using freeze-frame for detailed inspection or photography and then transferred to a computer for further image enhancement.

V. REPRESENTATIVE EXPERIMENTAL RESULTS

A. Metals

Figure 13 shows plateaus on a Au(100) surfaces separated by monatomic steps.³¹ The corrugations on the plateaus are due to a reconstruction. This reconstruction shows up in low-energy electron diffraction (LEED) patterns as shown in the inset. A similar reconstruction also occurs on the (100) surfaces of Pt and Ir.³²

Higher-resolution images³¹ showed that the reconstruction is not the same all over the plateaus. The tunneling microscope could detect subtle variations in the atom positions at different locations. For example, at some locations there were two rows of atoms at the top of the five-row corrugation pattern while at other locations there was only one row at the top.³¹ Careful analysis of these subtle variations leads to the conclusion that the Au(100) surface is covered by a slightly rotated (0.1°), isotropically contracted (by 3.82%) hexagonal top layer, forming an incommensurate Au-on-Au structure.

The ability of the tunneling microscope to see the subtle variations within surface reconstructions makes it an enormously powerful tool. We can expect it to be used by many groups to obtain definitive results on metal surface reconstructions in the future.

Figure 14 shows terraces separated by steps on a Ag(100) surface.³³ This image was obtained with a tunneling microscope designed to be rigid, with low thermal

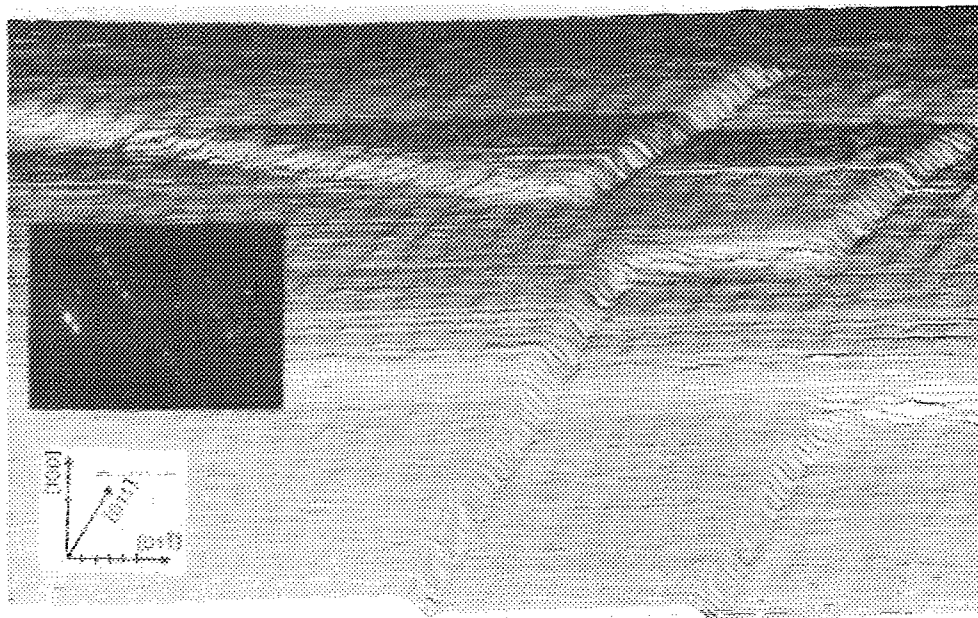


FIG. 13. Image of a clean reconstructed Au(100) surface with monatomic steps. The divisions on the crystal axes are 5 Å, with ≈ 1.5 Å from scan to scan. The second insert shows the LEED pattern of the predominant 1×5 corrugation. Figure from Binnig *et al.* (see Ref. 31).

Figure 15 shows terraces separated by steps on a Pd(100) surface.³⁴ These steps are closer than in Figs. 13 and 14 because the Pd crystal was tilted by 3.7° from the 100 direction.

A good study of the Pt(100) surface by Behm, *et al.*³⁵ shows not only terraces and steps, but also the reconstructions on the terraces. Of particular interest was that different terraces had reconstructions that were rotated with respect to each other. The reconstruction on a single terrace continued all the way to the boundaries of that terrace.

The (110) surfaces of noble metals have also been studied. In fact, images of the Au(110) surface appeared in the first paper on tunneling microscopy to show atomic steps and terraces.¹ A later, more detailed study⁹ of the terraces showed that a 1×2 reconstruction was driven by the formation of (111) facets.

The Au(110) surface was also used by Becker, Golovchenko, and Swartzentruber³⁶ for some elegant electron interferometry studies in which electron standing waves between the Au surface and a W tip were revealed by monitoring dI/dV versus bias voltage.

Figure 16 shows a Pt(110) surface with a large density of steps.³⁷ Features with 2- and 3-atom periodicity were de-

tected³⁷ over small areas, but the terraces were not large enough to reveal the details of the reconstructions.

Tunneling microscopy is also useful for characterizing evaporated metal films and polished, polycrystalline surfaces. Images of silver films by Raether³⁸ revealed roughness of about 5 Å obtained from the light emitted from the surface plasmons via roughness. Images of gold films by Drake *et al.*³⁹ revealed "rolling hills" with heights of order 50 Å and widths of order 200 Å.

Polished surfaces that are used as surface finish standards have also been imaged with a tunneling microscope by Garcia *et al.*⁴⁰ Roughness on a lateral scale too small to be revealed with conventional diamond stylus profiling instruments was clearly resolved with the tunneling microscope. This investigation was made with the tunneling microscope operating not in high vacuum, as for the studies discussed so far, but in air at atmospheric pressure!

More recently this same group has demonstrated imag-

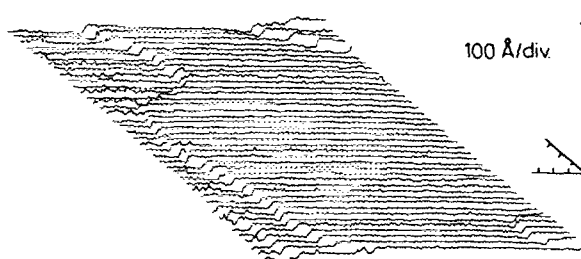


FIG. 14. Image of a Ag(100) surface. Again large flat terraces separated by steps can be seen. Figure from van de Walle *et al.* (see Ref. 33).

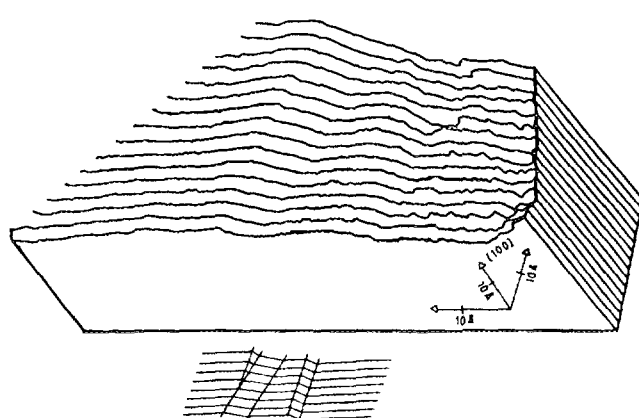


FIG. 15. Image of a Pd(100) surface. The inset is a model of the steps in the image. Figure from Ringger *et al.* (see Ref. 34).

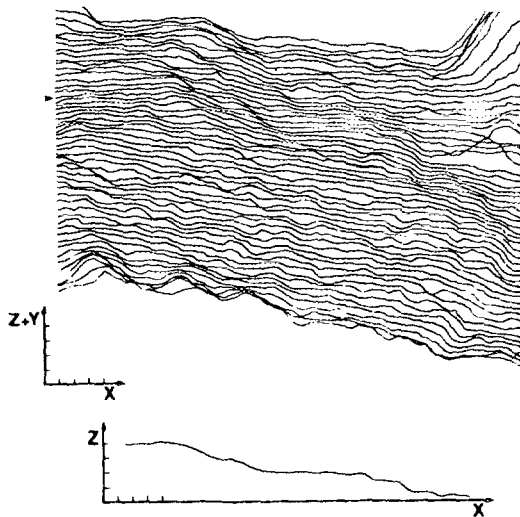


FIG. 16. Image of a Pt(110) surface. The single line scan shows steps and short terraces. The scale marks 4 Å. There is a separate line scan from the arrowed position. Figure from Pashley, Pethica, and Coombs (see Ref. 37).

ing in air of a variety of other surfaces⁴¹: a Au(100) single crystal, a Pt film on mica, a CdTe film on glass, and a TiO₂ oxide layer on polycrystalline Ti foil. They emphasize that it is possible to study technologically important surfaces under the actual conditions in which they will be used.

Figure 17 shows an example of using a tunneling microscope to study a surface in a technologically important environment: an aqueous solution.⁴² The gold surface was submerged in a dilute saline solution. A key to making the tunneling microscope work in a conductive solution was using a needle that was designed for intracellular recording and was covered with glass insulation except very near the tip. These needles are commercially available.⁴³ Operation in aqueous solutions opens new opportunities for research in electrochemistry and, possibly, biology.

Figure 18 shows that the electrical characteristics that

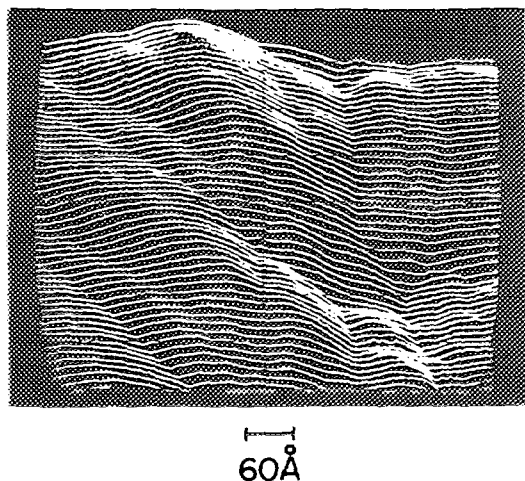


FIG. 17. Image of a thin film of gold covered with a 2-mM NaCl solution in water. Figure from Sonnenfeld and Hansma (see Ref. 42).

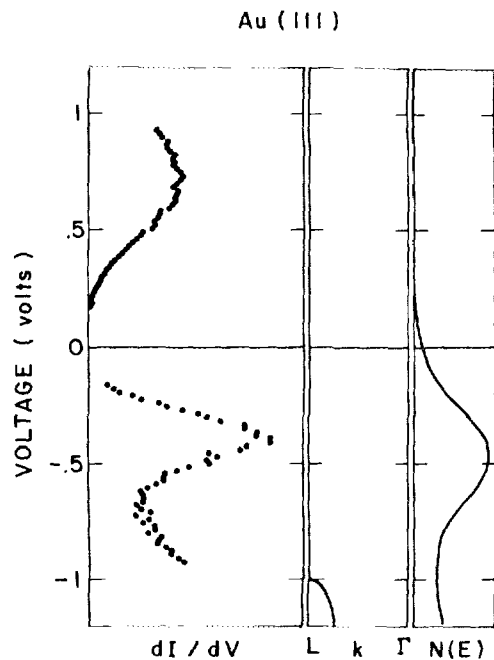


FIG. 18. (a) Conductance vs voltage plot for a Au(111) surface probed with a tungsten tip in a tunneling microscope. (b) The band structure for the Au. (c) Ultraviolet photoemission spectroscopy (UPS) result for the surface state on the Au. Figure from Kaiser and Jaklevic (see Ref. 44).

can be measured by hovering the tip of a tunneling microscope over one region of a sample contain information about the electronic states of the sample.⁴⁴ Specifically, in this case the surface state 0.4 eV below the Fermi level of a Au(111) plot of dI/dV versus voltage is clearly revealed. Spatially resolved spectroscopy on metal surfaces should be possible and is an opportunity for pioneering research.

B. Semiconductors

Semiconductor surfaces in general and semiconductor surface reconstructions in particular have been excellent subjects for investigations with tunneling microscopes. Much of the rapid growth in tunneling and microscopy can be traced to the pioneering work of Binnig, Rohrer, Gerber, and Weibel and the 7×7 reconstruction of Si(111) (Refs. 3 and 45). These first atomic resolution images not only contributed to the solution of a long standing problem in surface science, but also clearly demonstrated the potential of tunneling microscopy.

Figure 19 shows a particularly beautiful and informative image⁴⁶ of this famous reconstruction. Note that the reconstruction continues unmodified right up to step edges. This image was enhanced with an IRIS processor using curvature shading. Points with curvature downwards (lumps) are given light values while points with curvature upwards (pits) are given dark values.

Becker, Golovchenko, Hamann, and Swartentruber²⁸ have observed not only topology, but also surface states on the Si(111) 7×7 surface. The states' energies and strengths were strongly dependent on position in the unit mesh. More

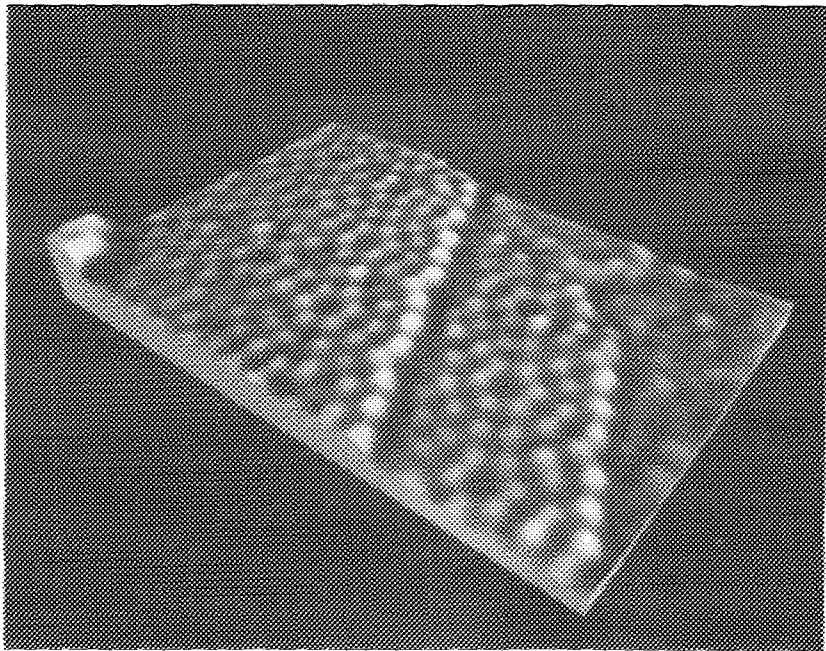


FIG. 19. Image of a Si(111) surface with 7×7 reconstructions on terraces that continue all the way to the atomic steps at their borders. Figure from Becker *et al.* (see Ref. 46).

recently, Hamers, Tromp, and Demuth⁴⁷ measured the electrical characteristics above each of the exposed atoms on this same surface. This type of spatially resolved spectroscopy has enormous potential for helping scientists and engineers to achieve a detailed understanding of the electronic properties of semiconductor surfaces on the microscopic scale.

As discussed in Sec. III and illustrated in Fig. 11, Tromp, Hamers, and Demuth²⁶ have also used tunneling microscope images to select the most likely model of the surface from many candidates. They show that the model of Takayanagi⁴⁸ fits their observed images best. Golovchenko came to the same conclusion and discusses it in a recent, excellent summary of results on the 7×7 reconstruction of the Si(111) surface.⁴⁹

Figure 20 shows that if silicon is cleaved to expose the (111) surface the reconstruction is 2×1 rather than 7×7 .⁵⁰ This 2×1 reconstruction is metastable and will convert to the 7×7 if the surface is annealed at 300–600 °C.⁵¹ The images of the 2×1 reconstruction support the π -bonded chain structure proposed by Pandey.^{52–54} Voltage dependence of the images revealed disorder-related surface states.⁵⁰ One of the authors of this paper, W. A. Thompson, anticipated the recent development of tunneling microscopy with his earlier work on direct vacuum tunneling.⁵⁵

Tromp, Hamers, and Demuth⁵⁶ also have imaged the (001) surface of Si and observed dimers. Both buckled and nonbuckled (symmetric) dimers are present, in roughly equal proportions, suggesting that their energies are nearly the same. The presence of the symmetric dimers shows up as a (2×1) diffraction pattern in LEED studies.⁵⁷ In some regions the buckled dimers were observed⁵⁸ to alternate in buckling direction. This would explain the $c(4 \times 2)$ and $p(2 \times 2)$ symmetries also previously observed with LEED⁵⁹ and helium scattering.⁶⁰

In addition to detailing the nature of the reconstructions on carefully prepared, flat semiconductor surfaces, tunnel-

ing microscopy can also reveal the nature of the microroughness on oxidized and ion-etched samples. Figure 21 is an image of a (100) silicon wafer that has not been ion etched.⁶¹ Figure 22 is an image of a similar sample after ion etching.⁶¹ Note the hillocks produced by the ion etching. An understanding of this type of microstructure may be of great importance as silicon technology is pushed to smaller and smaller structures.

Before leaving our discussion of silicon, it is worthwhile to mention one difficulty in studying lightly doped silicon in particular and poorly conducting samples in general. Flores and Garcia⁶² have discussed the voltage drop inside a semiconductor due to the spreading resistance. They calculated

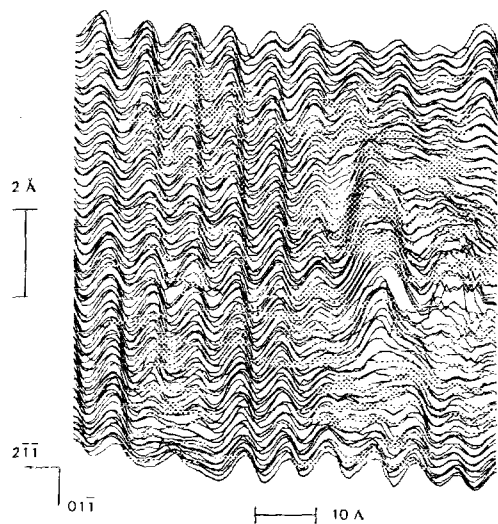


FIG. 20. Image of a cleaved Si(111) surface showing a 2×1 reconstruction on the left-hand side of a disordered region on the right. Figure from Feenstra, Thompson, and Fein (see Ref. 50).

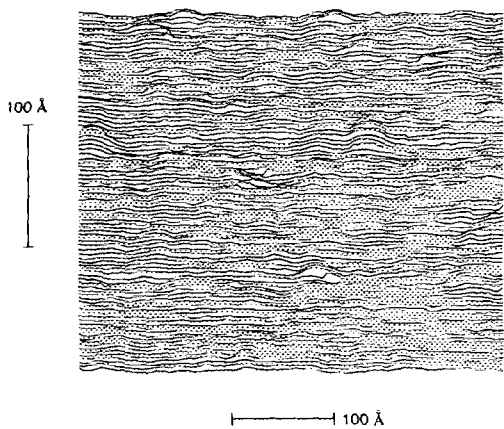


FIG. 21. Image of a mechanically polished, chemically etched Si(100) wafer. The rms roughness was measured to be 1.6 Å. Figure from Feenstra and Oehrlein (see Ref. 61).

that this voltage drop can be several tenths of a volt for resistivities in the range of a few $\Omega \text{ cm}$. These voltage drops could be especially serious for spectroscopy on high-resistivity samples.

Figure 23 shows the complex reconstruction on two terraces of a Ge(111) surface.⁶³ The basic symmetry of these reconstructions is $c2\times8$ with $p2\times2$ and $c4\times2$ subunits. Becker, Golovchenko, and Swartzentruber⁶³ also observed regions with 7×7 reconstructions similar to those on Si(111).

Compound semiconductors have also been studied. In one of the first papers on tunneling microscopy, Scheel, Binning, and Rohrer⁶⁴ presented images of GaAs(111) crystals grown by liquid-phase epitaxy. The images showed atomically flat terraces bounded by 6.5-Å-high steps.

Figure 24 shows more recent results on cleaved GaAs(110).⁶⁵ The surface had a 1×1 periodicity. The dark regions in the center and lower left of the image were associated with point defects.

Finally, Fig. 25 shows the surface of an alloy semicon-

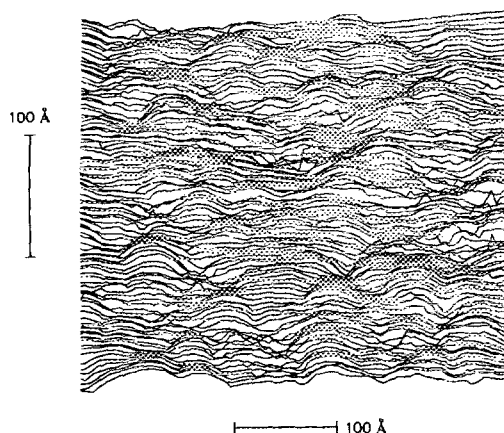


FIG. 22. Image of a mechanically polished, chemically etched Si(100) wafer after ion etching. The rms roughness was measured to be 4 Å. Figure from Feenstra and Oehrlein (see Ref. 61).

ductor: GeSi.⁶⁶ The 5×5 reconstruction on this (111) surface occurs at a stoichiometry of 50–50. It looks like a miniature version of the 7×7 reconstruction; the distance between the corner holes is shortened.

Thus tunneling microscopy can yield useful information on surface roughness, surface reconstructions, surface electronic states, and surface defects on a wide variety of semiconductors including compound semiconductors and alloys.

C. Superconductors and low-temperature spectroscopy

Ever since the Nobel-prize winning research of Giaever,⁶⁷ tunneling has been used to gain a detailed understanding^{68–70} of the superconducting state. Now, with tunneling microscopy, that understanding can be extended to include spatial variations in superconducting properties on a microscopic scale.

Figure 26 shows the first reported observation of superconducting energy gap measured with a tunneling microscope.⁷¹ The value for the gap of 3.7 meV is within the expected range, based on other measurements.⁷² The sample was a thin film of Nb₃Sn on a sapphire substrate. This film was cleaned with ion bombardment after deposition.

Figure 27 illustrates the potential of the tunneling microscope for studies of spatial variations of superconducting properties over microscopic lengths.⁷³ The ratio of the conductance at zero voltage to the conductance at voltages well above the superconducting gap voltage, $\sigma(V=0)/\sigma(V \gg \Delta)$, is a sensitive measure of the presence of superconductivity. For tunneling to a superconductor well below its transition temperature this ratio is near zero.^{67–70} For tunneling to a normal conductor this ratio is near one.^{67–70} Thus the spectroscopic image shown in Fig. 7(a) reveals that there is a normal region at one corner of an otherwise superconducting sample. The topographic image shown in Fig. 7(b) reveals a corresponding change in the surface roughness.

Additional research opportunities for tunneling microscopy at low temperature include phonon spectroscopy^{68–70} and perhaps even molecular vibration spectroscopy.^{69,74} With conductance stability of order 1% some phonons spectroscopy could be done. With stability of order 0.1% most phonon spectroscopy and some molecular vibrational spectroscopy could be done. Finally, with stability of order 0.01%, detailed molecular vibrational spectra could be obtained.

Figure 28 illustrates the type of phonon spectroscopy that has already been done on superconductors with another type of mechanically adjustable tunneling structure: the squeezable electron tunneling junction.^{75–77} In these junctions the ability to scan laterally was sacrificed to gain stability in the gap spacing. They had enough conductance stability for phonon spectroscopy in superconductors and normal metals, but not enough for molecular vibrational spectroscopy. More specifically, though the conductance was stable enough at low bias voltages there was an abrupt increase to unacceptable noise levels at bias voltages of roughly 40 mV.

It is, however, possible that most of the observed noise was due to the filling and emptying of localized electron

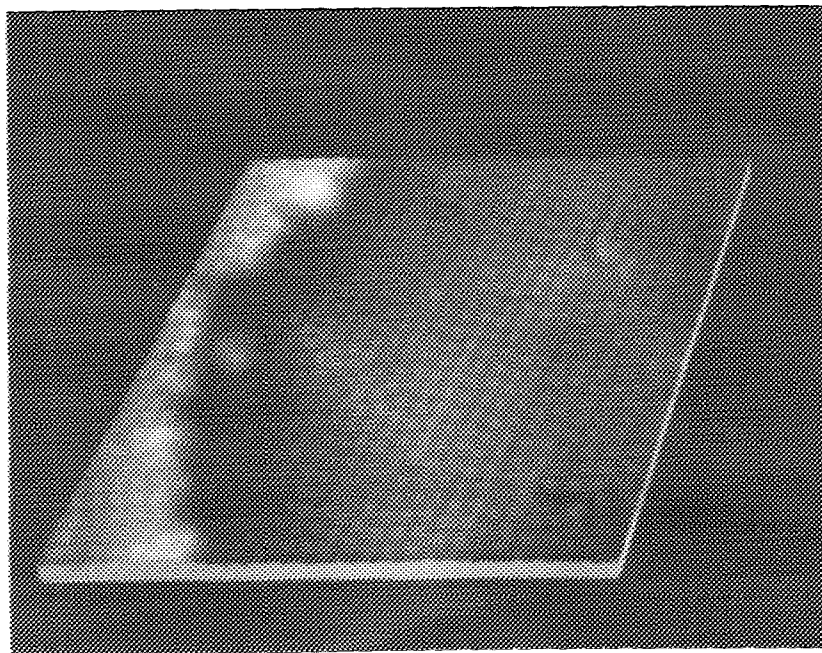


FIG. 23. Grey scale image of a Ge(111) surface with two terraces. The image was tilted and put in perspective by an IRIS processor. It is from Becker and Swartzentruber (see Ref. 63).

traps in thin oxide layers on the electrodes.⁷⁸⁻⁸⁰ If so, stable enough conductances may be achievable with future tunneling microscopes or squeezable junctions that have oxide-free electrodes.

If the excess noise, which is possibly due to localized electron traps, could be eliminated then some molecular vibrational spectroscopy should be possible. The intrinsic noise in high resistance tunnel junctions is dominated by shot noise⁸¹; the shot-noise voltage is $V_{sn} \approx \sqrt{2eVR\Delta f}$. For $V = 100$ mV, $R = 10$ MΩ, and $\Delta f = 1$ Hz, this gives $V_{sn} \approx 6 \times 10^{-7}$ V. Molecular vibrational spectra for oxide-barrier junctions are generally measured with a second harmonic voltage detection scheme^{69,74}; peak heights are in the range 10^{-8} – 5×10^{-6} V for a 2-mV modulation level. Thus the largest peaks^{82,83} would be almost an order of magnitude above the noise level in a 1-Hz bandwidth. Increasing the modulation level and decreasing the bandwidth would help in the observation of smaller peaks. The price paid would be less resolution and longer measuring times.

The importance of molecular vibrational spectroscopy is not that there is any great interest in the vibrations themselves, but rather that the vibrational spectrum reveals not only what molecules are present, but even the details of their bonding to a surface.⁶⁹ Thus if molecular vibrational spectroscopy were possible with a tunneling microscope it might be possible to do chemical analysis of adsorbed layers on a molecule by molecule basis.

D. Layered materials

1. Highly oriented pyrolytic graphite (HOPG)

Figure 29 shows experimental²⁹ and theoretical²² images of HOPG for comparison. In both images the dominant feature is a low spot (black) in the center of each graphitic ring. This is due to the low electron density there. The tip must dip close to the surface to maintain a constant tunneling current.

A more subtle feature of the images is the inequivalence of the surface carbon atoms that make up the graphitic rings. Surface carbon atoms that are not above carbon atoms in the

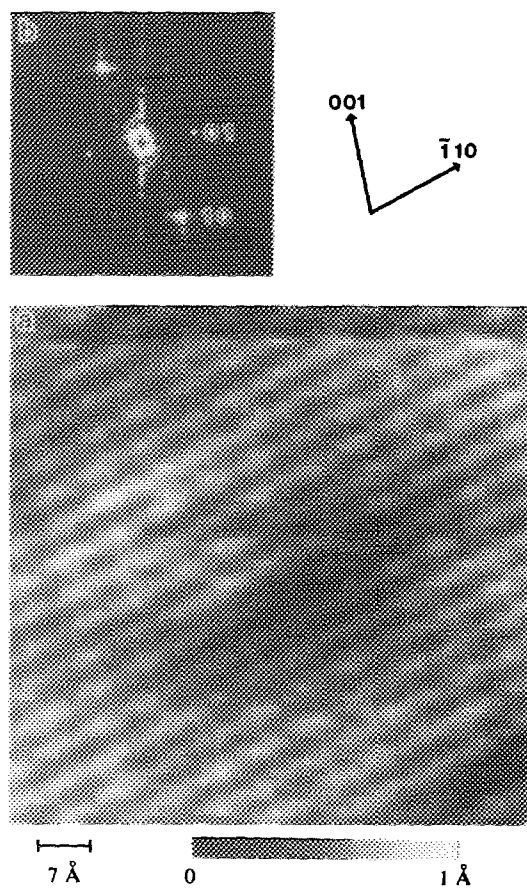


FIG. 24. Image of GaAs cleaved to expose a (110) plane. Zigzag chains of alternating Ga and As atoms directed in the (100) direction can be seen clearly. The insert shows a Fourier transform of the image. Figure from Feenstra and Fein (see Ref. 65).

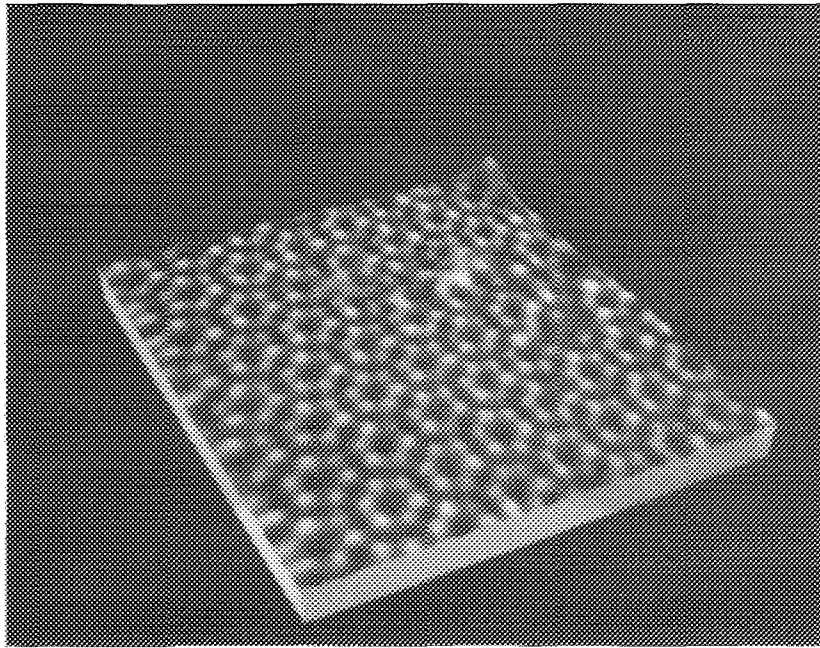


FIG. 25. Image of a layer of Ge-Si alloy grown on top of a Si(111) wafer. Figure from Becker, Golovchenko, and Swartzentruber (see Ref. 66).

second layer (black dots in the figure) have maxima over them (with spots). On the other hand, surface carbon atoms that are above carbon atoms in the second layer (white dots in the figure) do not have visible maxima over them. Here too experiment and theory are in agreement.

Figure 30 shows raw and digitally filtered images of HOPG taken in air at ambient pressure.⁸⁴ The digital filtering used the Wiener optimum filter⁸⁵ with the assumption that there was $1/f$ noise along the x axis and white noise along the y axis. These were the first published images to reveal that atomic-resolution tunneling microscopy was possible in air.

Figure 31 shows that it is even possible to obtain atomic-resolution images under water. Though this image was obtained under deionized water, Sonnenfeld⁸⁶ has more recent-

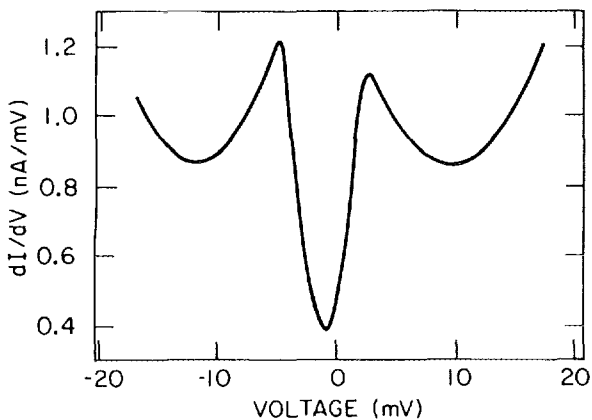


FIG. 26. Superconducting energy gap of a Nb₃Sn sample was revealed in this dI/dV vs voltage plot taken with the tip of a tunneling microscope hovering over one location on the sample. Figure from Elrod, de Lozanne, and Quate (see Ref. 71).

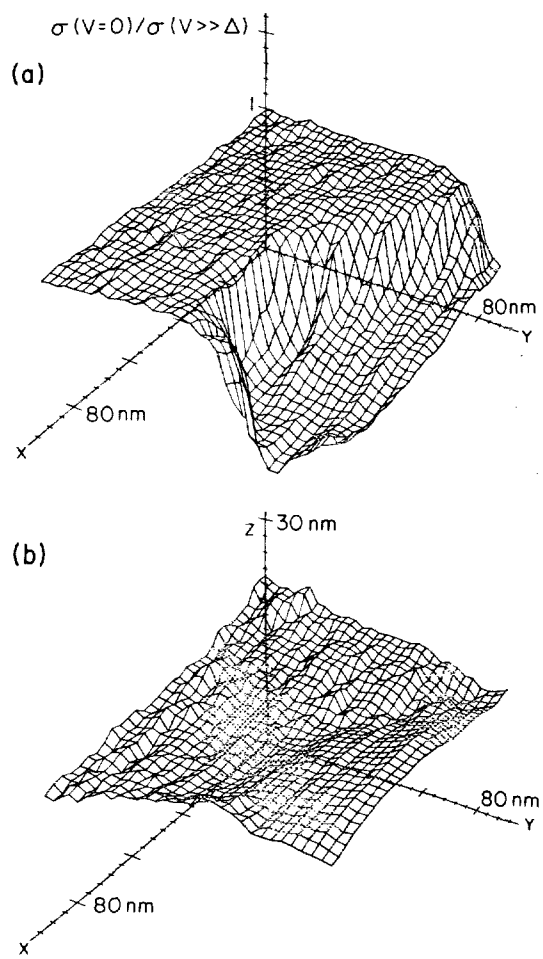


FIG. 27. (a) Image of the spatial variations in the superconducting properties of a Nb₃Sn sample. (b) Image of the topography of the same region taken at the same time. Figure from Elrod *et al.* (see Ref. 73).

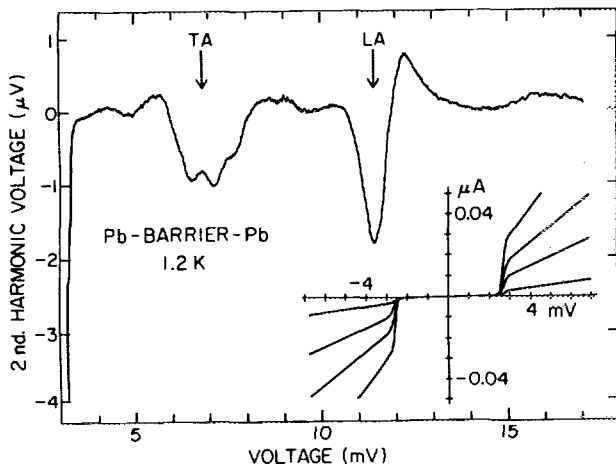


FIG. 28. Second-harmonic voltage vs bias voltage for a squeezable electron tunnel junction with superconducting lead electrodes. The insert shows current vs voltage curves obtained with different squeezing forces applied to the junction. Figure from Moreland and Hansma (see Ref. 76).

ly obtained atomic-resolution images even under a commercial gold plating solution.⁸⁷ Though tunneling microscopy in vacuum represents a real advance in analytical techniques it is, in some ways, in competition with electron microscopy, which also has atomic resolution.⁴⁶

In air at ambient pressure and in water there is no atomic-resolution competition. Most studies in these environments are done with optical microscopes, which reached their fundamental resolution limit of roughly 2000 Å by the 1890's. X-ray microscopy⁸⁸ has achieved a lateral resolution of 75 Å. In the future, lateral resolutions of 10 Å may be possible,⁸⁸ but atomic resolution seems unlikely. Thus, the atomic resolution that is now possible with tunneling mi-

croscopy opens unique opportunities for studies in these environments.

2. Transition-metal chalcogenides

One of the things that is becoming clearer is that scanning tunneling microscopy probes not the topology of a surface, but rather the topology of the electron distribution above the surface. The topology of the electron distribution above the surface usually follows the topology of the surface—but not always. For example, if a charge density wave is present on a surface, the topology of the electron distribution, and hence, tunneling microscope images,^{89,90} can be completely different, at least on an atomic scale, from the topology of the surface. More subtle examples are the nearly two-dimensional materials such as highly oriented pyrolytic graphite (HOPG) and transition-metal dichalcogenides without charge density waves. For these materials the electron distribution has the same periodicity as the surface topology, but the amplitude and shape of the features in the electron distribution, and hence in the tunneling microscope images^{21–27} can not only differ from the surface topology, but even have dramatic voltage dependencies.²⁴ These experimental results can now be understood with new theoretical work^{22,24} based on the original work of Tersoff and Hamann.^{13,14} The new work calculates the appropriate electron densities, and predicts tunneling microscope images in at least qualitative agreement with experiment.

Figure 32 compares images taken above different regions on 4Hb-TaS₂ immersed in liquid nitrogen.⁹⁰ Though all cleaved surfaces of 4Hb-TaS₂ are covered with close-packed sulfur atoms, the atoms are only visible in Fig. 32(a). Figure 32(b) is dominated by relatively high amplitude features with a lattice constant over three times as large as the lattice constant of the atoms.

The 4Hb phase of TaS₂ has four layers per unit cell with alternating layers of trigonal prismatic and octahedral coordination.⁹⁰ At 77 K only the octahedral layers support a charge density wave. Its wavelength is $\sqrt{13}$ times the atom spacing. Thus, if a trigonal prismatic layer were exposed one would expect to see only atoms. If an octahedral layer were exposed one would expect to see charge-density waves.

Figure 33 supports these ideas. The central terrace has a charge density wave and thus must be an octahedral layer.⁹⁰ If the terraces to the left- and right-hand side are one cleavage plane above and one cleavage plane below the central octahedral layer, then they would be trigonal prismatic layers without charge density waves as seen in the image. (Unfortunately there was not enough resolution in this image to clearly reveal the atoms on these layers.)

Coleman and his co-workers have also imaged 1T-TaS₂, 1T-TaSe₂, 2H-TaS₂, and 2H-TaSe₂.^{89,90} For example, Fig. 34 shows atoms and single atom defects on 2H-TaS₂. Immersion of this microscope³⁹ in liquid nitrogen helped decrease thermal drifts and provided an inert environment. Immersion in liquid helium should be even better for low-drift, high-resolution imaging. Could traces of the shapes of atomic orbitals be resolved? The answer should be known within the next few years.

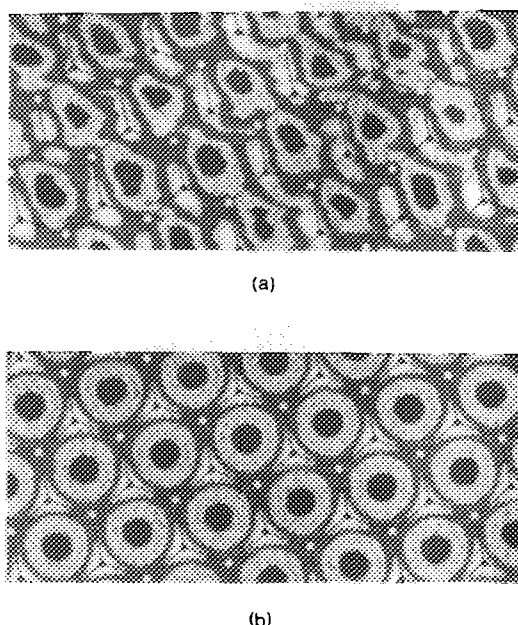


FIG. 29. (a) Grey scale image of highly oriented pyrolytic graphite (HOPG) in high vacuum. (b) Grey scale theoretical image based on the work of Selloni *et al.* (Ref. 22). Figure from Binnig *et al.* (see Ref. 29).

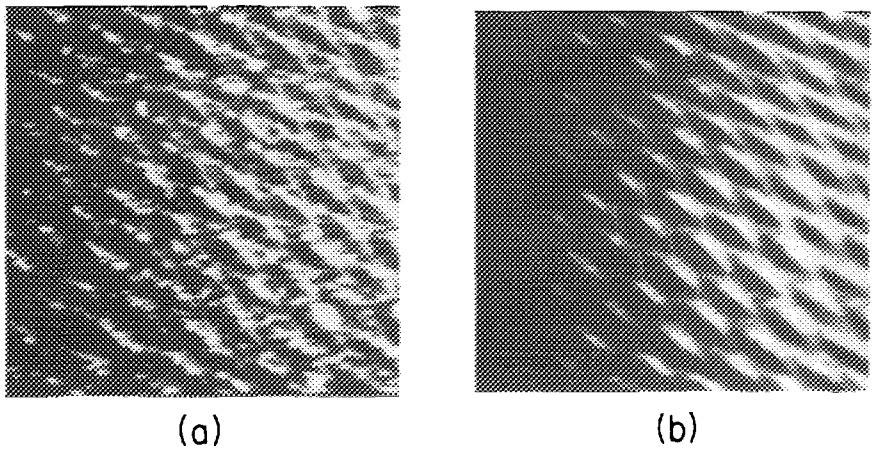


FIG. 30. Grey scale images of (a) raw data and (b) digitally filtered data for HOPG in air. The hexagonal grid is superimposed as an aid to visualization of the unit cell. Figure from Park and Quate (see Ref. 84).

E. Adsorbed molecules and biological materials

Figure 35 is an image⁹¹ of oxygen chemisorbed on Ni(110). The maxima (light regions) in ordered 2×1 domains were associated with individual oxygen atoms.⁹¹ The surface coverage of these maxima was determined by counting to be $\theta = 0.35$, in agreement with independent measurements^{92,93} of the saturation coverage of oxygen on Ni(110).

Though oxygen on Ni was the first published image of a surface with ordered, isolated adsorbate atoms, there are earlier images with structures probably due to adsorbates—even in one of the very first papers on tunneling microscopy.¹ In another early paper, Binnig *et al.*³¹ attributed hills on a Au(110) surface to carbon clusters one and two layers high based on the fine structure on the hills and the detection of carbon with AES.

Figure 36 is an image of DNA on a carbon substrate. This image is interesting for many reasons. It shows that some adsorbates are imaged as dips rather than peaks; the tip

dips toward the adsorbate rather than rising up over it. It shows that it is possible to operate a tunneling microscope with the tip tens of Angstroms (Binnig estimated 50 Å)⁹⁴ away from a surface since the tip was able to dip down to-

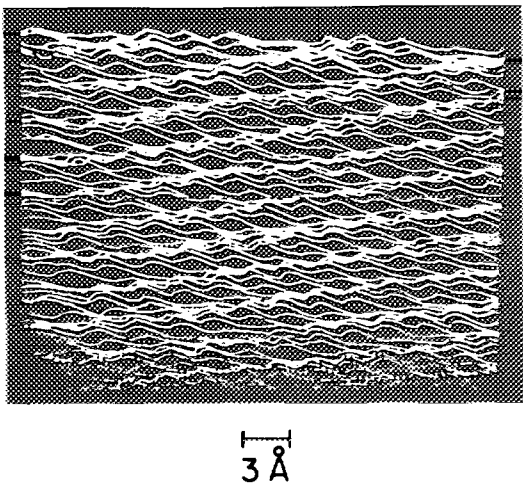
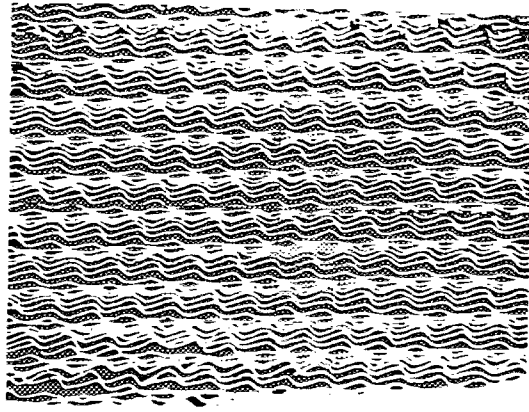


FIG. 31. Image of HOPG immersed in water. The hexagonal nature of the lattice in this line scan image can be seen by noting that the features line up in rows along three axes separated by about 120°. The imaging process emphasized the rows at a slight angle to horizontal and the rows falling at about 45° from upper left to lower right. A third set of rows may be seen that is nearly vertical but slopes to the right from bottom to top. Figure from Sonnenfeld and Hansma (see Ref. 42).

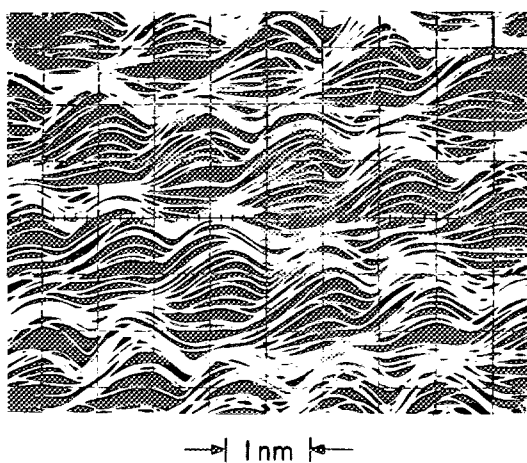


FIG. 32. Images of two regions on cleaved 4Hb-TaS₃ immersed in liquid nitrogen. (a) Sulfur atoms are revealed as bumps 3.29 ± 0.16 Å apart, presumably in regions where the trigonal prismatic layer is exposed. (b) Charge density waves are revealed as bumps 12.11 ± 0.12 Å apart, presumably in regions where the octahedrally coordinated layer is exposed. Figure from Slough *et al.* (see Ref. 90).

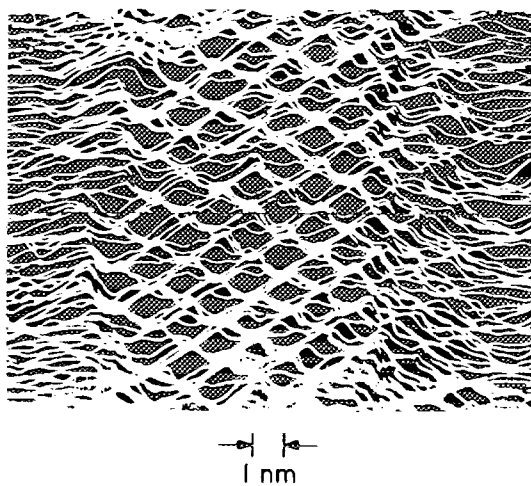


FIG. 33. Image of cleaved 4Hb-TaS₂ immersed in liquid nitrogen. Two steps separate the imaged region into three terraces. A charge-density wave is present on the central terrace, but not on the terraces to the right and left. Figure from Slough *et al.* (see Ref. 90).

ward the DNA and still not touch it, and, probably most importantly, it shows that tunneling microscopy may contribute to biology by supplying images of macromolecules.

Baró *et al.*⁹⁵ have shown that cleaved highly ordered pyrolytic graphite (see Sec. V D 1) is atomically flat over regions of order 1000 Å in lateral dimensions and thus can be used as a substrate for imaging biological structures. They have also⁹⁵ deposited bacteriophage ϕ 29 on a graphite surface from an aqueous solution, air-dried the surface, imaged it with a tunneling microscope, and compared their images to those from conventional electron microscopy.

There are definite similarities between the structures reported for the two techniques.⁹⁵ Further research will determine the reproducibility of this pioneering work and the mechanism of imaging. For example, one thing that is still mysterious at this time is why the tunneling tip apparently

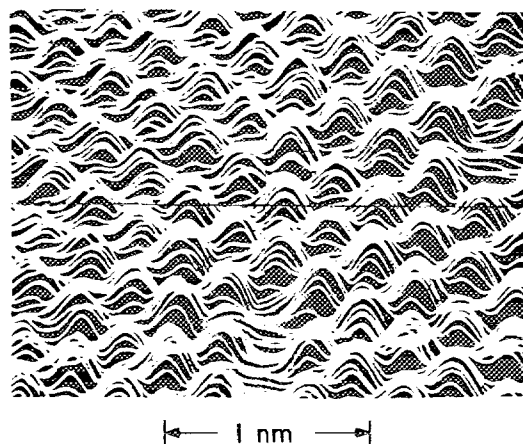


FIG. 34. Image of atoms on cleaved 2H-TaS₂ immersed in liquid nitrogen. Note the single-atom defects near the center of the bottom border and on the right border. Figure from Slough *et al.* (see Ref. 90).

went up and over the ϕ 29 rather than dipping toward it as for the DNA. Perhaps enough water of hydration was retained by the ϕ 29 after air drying to make it somewhat conductive, but this is only speculation at present.

The ability to image macromolecules will be especially significant if they can be imaged in their fully hydrated, biologically active state. As mentioned before, tunneling microscopy in vacuum competes with other types of electron microscopy. These have already made important contributions to the imaging of biologically significant structures in the dehydrated state—with inferences, based on elegant experimental techniques to what they must have been like in the hydrated state. Still, it would be at least comforting and possibly very revealing to actually image structures in the fully hydrated, biologically active state. Fast imaging in the hydrated, active state may also open the door to imaging of biological processes in real time.

Progress in this direction has already been made. As mentioned previously, fast imaging⁵ and imaging of surfaces under aqueous solutions⁴² have already been accomplished. More recently, fast imaging of a lipid bilayer at molecular resolution has been reported.⁹⁶ The bilayer was of cadmium arachidate on a graphite surface. The molecular spacing was measured to be 4.9 Å, in agreement with electron diffraction data.

F. Lithography

Figure 37 shows that some lithography can be done by simply scratching the surface with the tip of the STM.⁹⁷ The same group also found that it was possible to deposit material from the tip onto the surface. Thus it was possible to use the tip both to remove and to deposit material. Surface diffusion could be observed with the STM on a time scale of minutes after material was transferred.

Figure 38 shows lines with an average spacing of 160 Å drawn with an STM on glassy Pd₈₁Si₁₉ (Ref. 98). It was proposed that these lines are composed of carbonaceous material polymerized by the STM tip from the hydrocarbon film that covered the surface. The presence of the hydrocarbon film was known from XPS measurements.

Ringer *et al.*⁹⁸ also proposed that conducting lines could be deposited by operating at STM in a gas containing main group alkyl compounds or transition metal alkoxy complexes. These materials would be decomposed electrically under the STM tip and deposit metals on the substrate.

More recently, McCord and Pease,⁹⁹ who are experts in electron-beam lithography, have begun work on STM lithography. They used the STM tip to expose both “contamination” resist (composed of hydrocarbon contamination) and a thin Langmuir–Blodgett film of docosanoic acid. They produced lines spaced roughly 1 μm apart with widths of order 0.1 μm with both resists, but the “contamination” resist gave better results. They proposed that chalcogenide inorganic resist systems¹⁰⁰ and metal halide resist systems¹⁰¹ might be useful in future research and mentioned that much improvement in writing speed would be necessary for device manufacturing.

Clearly the STM has the potential for doing state of the

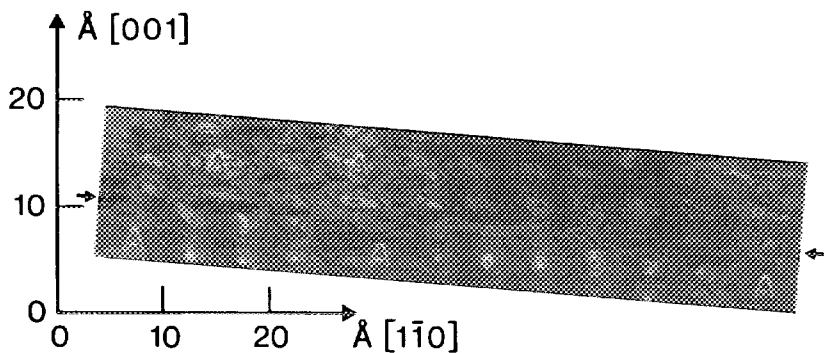


FIG. 35. Contour image of oxygen chemisorbed on Ni(110). The contours of equal corrugation height are spaced 0.1 Å apart in the lower, and 0.05 Å apart in the upper part. The lower resolution in the upper part is presumably due to a change in the tip condition while the image was being obtained. The regions of 2×1 structures are separated by wide domain walls (marked with A's). Figure from Baró *et al.* (see Ref. 91).

art lithography. Speculations on longer-term implications of the pioneering work discussed here follow in Sec. VI.

VI. SPECULATIONS ON THE FUTURE

Some of the future is relatively easy to see. Established groups in the area of surface science will add STM to their alphabet soup of techniques: AES, LEED, UPS, XPS, TPD, *et al.* This is, for example, what has happened to high-resolution electron energy-loss spectroscopy (HREELS) over the past 10 years. The availability of commercial apparatus¹⁰² will accelerate the process. More possibilities for the future have been discussed at the end of the various subsections in Sec. V.

The rest of the future, though more difficult to see, is more interesting to contemplate. In a remarkably farsighted paper written over 25 years ago, Feynman¹⁰³ proposed that: "There's Plenty of Room at the Bottom." He saw that we were far from any natural limits to miniaturization in many areas such as computers and machine tools.

He pointed out that miniaturized devices would have an enormous number of technical applications.¹⁰³ For example, it "would be interesting in surgery if you could swallow the

surgeon."¹⁰³ If we can arrange atoms and molecules the way we want "we will get an enormously greater range of possible properties that substances can have, and of different things that we can do."¹⁰³

More recently, he presented arguments that "the law of physics present no barrier to reducing the size of computers until bits are the size of atoms, and quantum behavior holds dominant sway."¹⁰⁴

Conrad Schneiker foresees a "NanoIndustrial Revolution" based on "nanotechnology" made possible by scanning tunneling microscopes and their descendants.¹⁰⁵ He discusses applications to computers, medicine, optics, materials research, and other fields. He even offers prizes to stimulate further miniaturization of STMs: "The challenges are to construct, operate, and publicly demonstrate STMs (including the mechanical positioning and scanning system), which can be controlled from the outside and which (not counting lead-in wires, fiber optics, etc.) are of the following sizes or smaller: (1 mm)³, (100 μm)³, (10 μm)³, (1 μm)³, (100 nm)³, and (10 nm)³... . The prizes, one per category, are currently \$1,000."

A key to many of the possible future applications of tunneling microscopy will be the development of the capacity to manipulate atoms and molecules with the tip. The lithography discussed in Sec. V F is a start. Gomer¹⁰⁶ has even calculated rates for various mechanisms of transferring atoms from or to the tip. Future possibilities include tips terminated with enzymes or antibodies to do biochemical operations. The point is that even some current STMs have enough stability to position and hold a tip over individual atoms. The tip can be thought of as a miniature robot arm—but one that currently lacks a hand.

Ideally, the hand should not only be able to grasp, but also to feel. Pressure sensitive transducers that give robot hands the ability to feel when they contact an object and then grasp it with a specified force have been a major advance in robotics. Though it may sound too wonderful to be true, progress has already been made in giving a scanning microscope the ability to feel a surface with its tip.

Binnig, Quate, and Gerber¹⁰⁷ have proposed a scanning microscope that can feel forces of order the interatomic force between two atoms. They have given sample calculations of what should be possible with relatively straightforward applications of current microfabrication technology and find

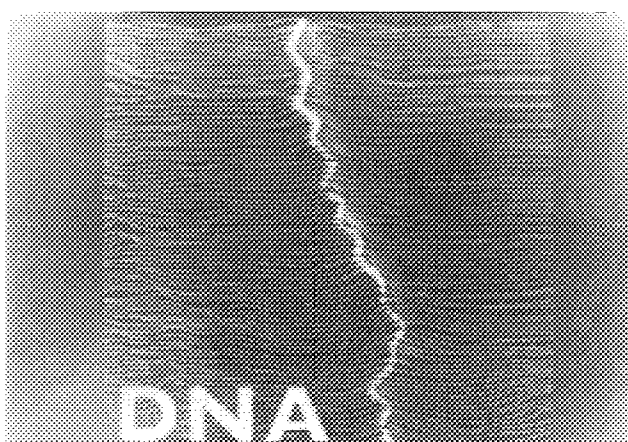


FIG. 36. Upside-down image of DNA on a carbon substrate. The wavelength of the zigzag is 35 ± 5 Å, roughly equal to the twisting periodicity of the double helix. The tip of the tunneling microscope dipped down toward the DNA. Therefore, the image was turned upside down because a long mound is easier to visualize than a long trough. Figure from Binnig (see Ref. 94).

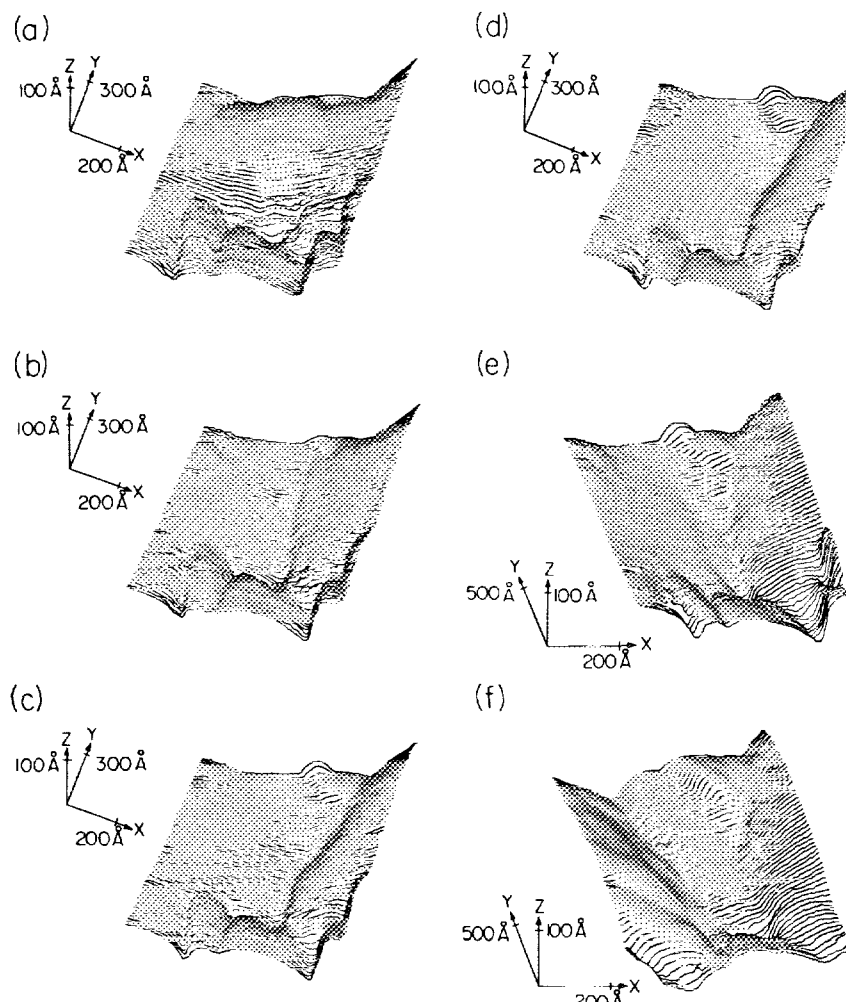


FIG. 37. Image of a gold film that has been scratched with the tip of a tunneling microscope: (a) shows the original topology; (b), (c), and (d) show successive images after scratching; (e) shows a rotated view; and (f) shows the rotated view after adding another scratch. Figure from Abraham *et al.* (see Ref. 97).

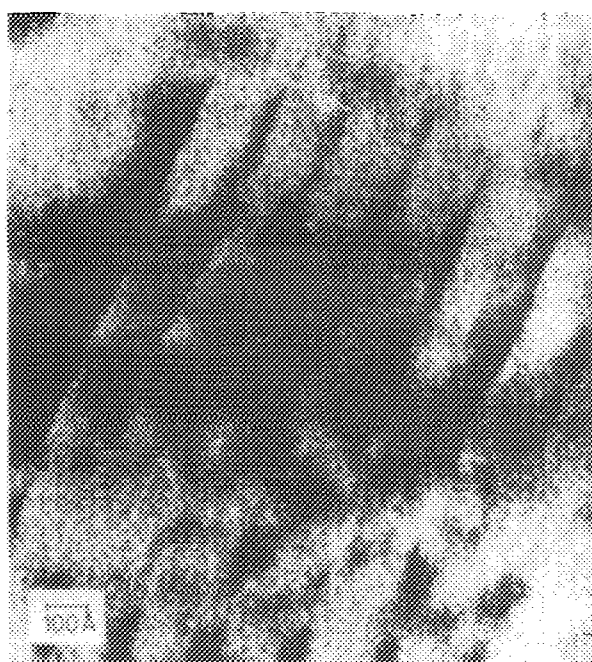


FIG. 38. Image of a glassy $\text{Pd}_{81}\text{Si}_{19}$ surface with freshly drawn lines. The asymmetry of the lines is attributed to the geometry of the tip used. Figure from Ringer *et al.* (see Ref. 98).

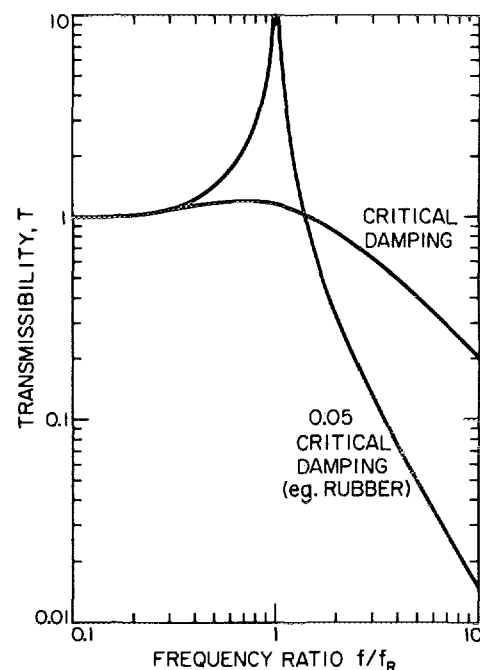


FIG. 39. Transmissibility T vs frequency ratio f/f_R for a critically damped and 0.05 critically damped system. Note that the price one pays for attenuation of vibrations above the resonant frequency is an amplification of vibrations near the resonant frequency.

that an "atomic force microscope," as they have christened it, should be possible to build. They even built a simple prototype using gold foil for a spring and a diamond tip. Their proposed model with a spring mass of 10^{-10} kg and a resonant frequency greater than 2 kHz should be able to scan a surface while negligibly deforming it.

The immediate application for an atomic force microscope is surface topography of insulator surfaces, which cannot be studied with STMs.

Another recent development with implications for the future is the use of a scanning tunneling microscope to plot potential distributions across a sample with microscopic resolution. Muralt and Pohl¹⁰⁸ used an ac bias voltage and corresponding ac tunneling current to set the distance above the surface and thus follow surface topography. There was also a dc voltage drop from one end of the sample to the other. The tip came to nearly the dc voltage of the part of the sample directly under it with the flow of dc tunneling current. Thus the surface topography and potential distribution could be measured at the same time.

Further information on tunneling microscopy and its bright future can be obtained from overviews of the field that have been published elsewhere.¹⁰⁹⁻¹¹⁴

VII. SUMMARY

(1) Lateral resolution is now sufficient to resolve protruding atoms on reconstructed surfaces and close-packed atoms on layered materials. Carbon atoms separated by 2.46 Å have been clearly resolved on graphite by several groups.

(2) Vertical resolution is now sufficient to resolve height differences as small as 0.02 Å in surface reconstructions.

(3) STMs have already been operated in vacuum, air, oil, liquid nitrogen, and water. They can probably be operated in most gases and liquids.

(4) STM has already been a powerful tool for studying a few surface reconstructions. Tens or hundreds of surface reconstructions will probably be studied within the next 10 years.

(5) Lithography with STMs has already produced lines separated by 160 Å. The potential for atomic scale manipulation exists.

(6) A few laboratories have begun exploring the potential of STM for biological materials. Operation under water may give STM an important advantage over conventional electron microscopy. Especially intriguing is the possibility of studying biological processes such as DNA replication.

ACKNOWLEDGMENTS

We thank Dr. D. Aspnes, Dr. J. Balodeschiwiler, Dr. R. Becker, Dr. K. Besocke, Dr. G. Binnig, Dr. J. Behm, Dr. R. Celotta, Dr. R. Coleman and his students, Dr. S. Chiang, Dr. J. Clarke and his students, Dr. J. Demuth, Dr. K. Dransfeld, Dr. R. Feenstra, Dr. H. Fink, Dr. N. Garcia, Mr. Ch. Gerber, Dr. J. Golovchenko, Dr. H. Güntherodt, Dr. R. Jaklevic, Dr. W. Kaiser, Dr. J. Kirtley, Dr. N. Lang, Dr. O. Marti, Dr. J. Pethica, Dr. D. Pohl, Dr. C. Quate and his students, Dr. H. Rohrer, Dr. C. Schneiker, Dr. A. Selloni, Dr. R. Tromp, Dr. H. Van Kempen, Dr. R. Wilson, Dr. R.

Young, and others for helpful discussions and for contributing material for this review. The research of one of us (P.K.H.) is supported by National Science Foundation Grant no. DMR 83-03623 and in part by the Office of Naval Research.

APPENDIX: VIBRATIONAL ISOLATION

Each stage of a vibration isolation system consists of elastic materials (e.g., springs or pieces of rubber) supporting a mass m . It can be characterized by a resonant frequency f_R . As shown in Fig. 39 there are three regions of frequency: (1) well below the resonant frequency the vibration isolation does nothing, vibrations are transmitted with just a little amplification; (2) near the resonant frequency vibrations are amplified substantially; and (3) well above the resonant frequency vibrations are attenuated.

You can easily strengthen your intuition for these three regions right now by holding a rubber band in your hand and hanging a weight (e.g., a pair of scissors) from it. As you move the top of the rubber band up and down slowly the weight moves with nearly the same amplitude as your hand, as you move it near the resonant frequency the weight moves with greater amplitude, and finally, if you vibrate your hand up and down very rapidly the weight will only move a little.

The amount of amplification near resonance and attenuation above resonance depends on the damping. As shown in Fig. 39, for critical damping the amplification has a maximum of less than 1.5, but then the attenuation is only a factor of 5 for a frequency 10 times the resonant frequency. Typical rubber has a damping of order 0.05 of critical. This gives an amplification of 10 near resonance, but an attenuation of over 50 for a frequency 10 times the resonant frequency. Typical undamped steel springs have a damping of order 0.005 of critical. This gives an amplification of 100 near resonance and an attenuation of roughly 100 for a frequency 10 times its resonant frequency. Thus some damping is desirable—for the extra factor of 2 attenuation by undamped steel springs at $10f_R$ the price is a factor of 10 more amplification near resonance—but critical damping is usually too much. Between 0.2 and 0.02 of critical damping is often a good range. The lower the resonant frequency relative to frequencies of interest, the less damping is necessary.

Thus, other things being equal, it is desirable to have as low a resonant frequency as possible. Figure 40 shows the resonant frequency f_R as a function of static deflection of the elastic materials, Δ . It is given by the formula

$$f_R = (1/2\pi) \sqrt{g/\Delta} = 0.5 \text{ Hz} \sqrt{1/\Delta} (\text{in meters}).$$

It is at first surprising, but nevertheless true, that the resonant frequency depends on the mass and spring constant only in this way; a car that deflects its suspension by 5 cm will have the same resonant frequency as a pair of scissors that stretches a rubber band 5 cm. It is worth noting that elastic supports with static deflections in the range 0.1–1 mm must be avoided. They will amplify vibrations right in the range in which building vibrations are most troublesome already. For other types of support such as in air-supported tables, more complex formulas apply.^{115,116}

The quality of vibration isolation can be quantitatively

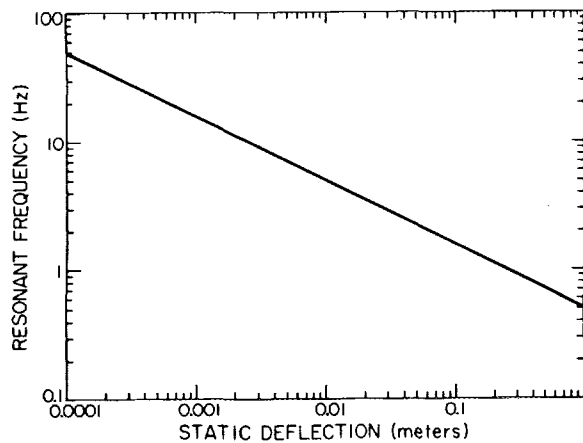


FIG. 40. Resonant frequency for an object that stretches (or compresses) its elastic supports by a given static deflection can be read from this graph. Note that resonant frequencies below 1 Hz require static deflections above 0.1 m.

evaluated with an inexpensive geophone as manufactured for oil exploration (e.g., L15B for under \$50 from Mark Products, Houston). This manufacturer recommends, for testing geophones, a basic vibration isolation system that we have found to be convenient and effective. Simply hang a large mass (a block of concrete is excellent) by rubber rod, tubing or aircraft landing gear shock cord from the ceiling. The rubber should stretch at least one yard to give a resonant frequency below 1 Hz.

Alternately one can use commercial air supported tables as manufactured primarily for optical applications (e.g., from Barry Controls, Watertown, MA). It is important for any vibration isolation system, and especially for these tables, to get the center of mass of the supported mass as low as possible relative to the supports; it does not work well to simply place a heavy vacuum chamber on top of a standard table.

The two systems can attenuate vibrations at 20 Hz (a typical building vibration frequency) by of order 100. It is important to note, however, that these relatively large systems are not necessary for atomic resolution microscopy. Several groups have operated microscopes with compact vibration isolation systems and done without isolation at low frequencies. It is a question of how quiet the laboratory environment is, how rigid the microscope is, and how much distortion of images one can tolerate in a given experiment.

¹G. Binnig, H. Rohrer, Ch. Gerber, and E. Weibel, Phys. Rev. Lett. **49**, 57 (1982).

²G. Binnig and H. Rohrer, Surf. Sci. **126**, 236 (1983).

³G. Binnig, H. Rohrer, Ch. Gerber, and E. Weibel, Phys. Rev. Lett. **50**, 120 (1983).

⁴A. Bryant, D. P. E. Smith, and C. F. Quate, Appl. Phys. Lett. **48**, 832 (1986).

⁵G. Binnig and D. P. E. Smith (unpublished).

⁶D. W. Abraham, H. Jonathon Mamin, Eric Ganz, and J. Clarke, IBM J. Res. Develop. **30**, 441 (1986).

⁷G. Binnig and H. Rohrer, Physica **127B**, 37 (1984).

⁸G. Binnig, H. Rohrer, Ch. Gerber, and E. Weibel, Appl. Phys. Lett. **40**, 178 (1981).

⁹G. Binnig, H. Rohrer, Ch. Gerber, and E. Weibel, Surf. Sci. **131**, L379 (1983).

¹⁰A. M. Baró, G. Binnig, H. Rohrer, Ch. Gerber, E. Stoll, A. Baratoff, and F. Salvan, Phys. Rev. Lett. **52**, 1304 (1984).

¹¹R. Young, Phys. Today **24**, 42 (1971).

¹²R. Young, J. Ward, and F. Scire, Rev. Sci. Instrum. **47**, 1303 (1976).

¹³J. Tersoff and D. R. Hamann, Phys. Rev. Lett. **50**, 25 (1983).

¹⁴J. Tersoff and D. R. Hamann, Phys. Rev. B **31**, 2 (1985).

¹⁵T. E. Feuchtwang, P. H. Cutler, and N. M. Miskovsky, Phys. Lett. **99A**, 167 (1983).

¹⁶A. Baratoff, Physica (Utrecht) **127B**, 143 (1984).

¹⁷N. D. Lang, Phys. Rev. Lett. **55**, 230 (1985).

¹⁸N. D. Lang, Phys. Rev. Lett. **56**, 1164 (1986).

¹⁹N. Garcia, C. Ocal, and F. Flores, Phys. Rev. Lett. **50**, 2002 (1983).

²⁰E. Stoll, A. Baratoff, A. Selloni and P. Carnevali, J. Phys. C **17**, 3073 (1984).

²¹J. Bardeen, Phys. Rev. Lett. **6**, 57 (1961).

²²A. Selloni, P. Carnevali, E. Tosatti, and C. D. Chen, Phys. Rev. B **31**, 2602 (1985).

²³E. Stoll, Surf. Sci. **143**, L411 (1984).

²⁴J. Tersoff, Phys. Rev. Lett. **57**, 440 (1986).

²⁵J. Tersoff, M. J. Cardillo, and D. R. Hamann, Phys. Rev. B **32**, 5044 (1985).

²⁶R. M. Tromp, R. J. Hamers, and J. E. Demuth, Phys. Rev. B **34**, 1388 (1986).

²⁷G. Binnig, Bull. Am. Phys. Soc. **30**, 251 (1985).

²⁸R. S. Becker, J. A. Golovchenko, D. R. Hamann, and B. S. Swartzentruber, Phys. Rev. Lett. **55**, 2032 (1985); R. J. Hamers, R. M. Tromp, and J. E. Demuth, Phys. Rev. Lett. **56**, 1972 (1986).

²⁹G. Binnig, H. Fuchs, Ch. Gerber, H. Rohrer, E. Stoll, and E. Tosatti, Europhys. Lett. **1**, 31 (1986).

³⁰G. Binnig and D. P. E. Smith, Rev. Sci. Instrum. (in press).

³¹G. Binnig, H. Rohrer, Ch. Gerber, and E. Stoll, Surf. Sci. **144**, 321 (1984).

³²M. A. van Hove, R. J. Koestner, P. C. Stair, J. P. Bibérian, L. L. Kesmodel, I. Bartos, and G. A. Somerjai, Surf. Sci. **103**, 189, 218 (1983).

³³G. F. A. van de Walle, J. W. Gerritsen, H. van Kempen, and P. Wyder, Rev. Sci. Instrum. **56**, 1573 (1985).

³⁴M. Ringger, H. R. Hidber, R. Schlögl, P. Oelhafen and H. J. Güntherodt, in *Proceedings of the 17th International Conference on Low-Temperature Physics*, edited by U. Eckern, A. Schmid, W. Weber, and H. Wüdl (Elsevier, Amsterdam, 1984), p. AF4.

³⁵R. J. Behm, W. Hösl, E. Ritter, and G. Binnig, Phys. Rev. Lett. **56**, 228 (1986).

³⁶R. S. Becker, J. A. Golovchenko, and B. S. Swartzentruber, Phys. Rev. Lett. **55**, 987 (1985).

³⁷M. D. Pashleyk, J. B. Pethica, and J. Coombs, Surf. Sci. **152/153**, 27 (1985).

³⁸H. Raether, Surf. Sci. **140**, 31 (1984).

³⁹B. Drake, R. Sonnenfeld, J. Schneir, P. K. Hansma, G. Slough, and R. V. Coleman, Rev. Sci. Instrum. **55**, 441 (1986).

⁴⁰N. Garcia, A. M. Baró, R. Miranda, H. Rohrer, Ch. Gerber, R. Garcia Cantu, and J. L. Peña, Metrologia **21**, 135 (1985).

⁴¹R. Miranda, N. Garcia, A. M. Baró, R. Garcia, J. L. Peña, and H. Rohrer, Appl. Phys. Lett. **47**, 367 (1985).

⁴²R. Sonnenfeld and P. K. Hansma, Science **232**, 211 (1986).

⁴³Part number 30-05-1 from Frederick Haer and Co., Brunswick, ME.

⁴⁴W. J. Kaiser and R. C. Jaklevic, IBM J. Res. Develop. **30**, 411 (1986).

⁴⁵G. Binnig, H. Rohrer, F. Salvan, Ch. Gerber, and Baró, Surf. Sci. **157**, L373 (1985).

⁴⁶R. S. Becker, J. A. Golovchenko, E. G. McRae, and B. S. Swartzentruber, Phys. Rev. Lett. **55**, 2028 (1985).

⁴⁷R. J. Hamers, R. M. Tromp, and J. E. Demuth, Phys. Rev. Lett. **56**, 1972 (1986).

⁴⁸K. Takayanagi, Ultramicrosc. **16**, 101 (1985).

⁴⁹J. A. Golovchenko, Science **232**, 48 (1986).

⁵⁰R. M. Feenstra, W. A. Thompson, and A. P. Fein, Phys. Rev. Lett. **56**, 608 (1986).

⁵¹R. Feenstra (private communication).

⁵²K. C. Pandey, Phys. Rev. Lett. **47**, 1913 (1981).

⁵³K. C. Pandey, Phys. Rev. Lett. **49**, 223 (1982).

⁵⁴K. C. Pandey, Proc. Indian Natl. Sci. Acad. Part A **51**, 17 (1985).

⁵⁵W. A. Thompson and S. F. Hanrahan, Rev. Sci. Instrum. **47**, 1303 (1976).

⁵⁶R. M. Tromp, R. J. Hamers, and J. E. Demuth, Phys. Rev. Lett. **55**, 1303 (1985).

- (1985).
- ⁵⁷R. E. Schlier and H. E. Farnsworth, in *Semiconductor Surface Physics*, edited by R. H. Kingston (University of Pennsylvania Press, Philadelphia, PA, 1957), p. 3.
- ⁵⁸R. J. Hamers, R. M. Tromp, and J. E. Demuth, Bull. Am. Phys. Soc. **31**, 226 (1986).
- ⁵⁹T. D. Poppdieck, T. C. Ngoc, and W. B. Webb, Surf. Sci. **75**, 287 (1978).
- ⁶⁰M. J. Cardillo and G. E. Becker, Phys. Rev. B **21**, 1497 (1980).
- ⁶¹R. M. Feenstra and G. S. Oehrlein, Appl. Phys. Lett. **47**, 98 (1985).
- ⁶²F. Flores and N. Garcia, Phys. Rev. B **30**, 2289 (1984).
- ⁶³R. S. Becker, J. A. Golovchenko, and B. S. Swartzentruber, Phys. Rev. Lett. **54**, 2678 (1985).
- ⁶⁴H. J. Scheel, G. Binnig, and H. Rohrer, J. Cryst. Growth **60**, 199 (1982).
- ⁶⁵R. M. Feenstra and A. P. Fein, Phys. Rev. B **32**, 1394 (1985).
- ⁶⁶R. S. Becker, J. A. Golovchenko, and B. S. Swartzentruber, Phys. Rev. B **32**, 8455 (1985).
- ⁶⁷I. Giaever, Rev. Mod. Phys. **46**, 245 (1974), his Nobel Prize acceptance speech.
- ⁶⁸E. L. Wolf, *Principles of Electron Tunneling Spectroscopy* (Oxford University Press, New York, 1985).
- ⁶⁹P. K. Hansma, ed., *Tunneling Spectroscopy: Capabilities, Applications, and New Techniques* (Plenum, New York, 1982).
- ⁷⁰W. L. McMillan and J. M. Rowell, in *Superconductivity*, Vol. 1, edited by R. D. Parks (Dekker, New York, 1969).
- ⁷¹S. A. Elrod, A. L. de Lozanne, and C. R. Quate, Appl. Phys. Lett. **45**, 1240 (1984).
- ⁷²D. A. Rudman, F. Hellman, R. H. Hammond, and M. R. Beasley, J. Appl. Phys. **55**, 3544 (1984).
- ⁷³S. A. Elrod, A. Bryant, A. L. de Lozanne, S. Park, D. Smith, and C. F. Quate, IBM J. Res. Develop. **30**, 387 (1986).
- ⁷⁴R. C. Jaklevic and J. Lambe, Phys. Rev. Lett. **17**, 1139 (1966).
- ⁷⁵J. Moreland, S. Alexander, M. Cox, R. Sonnenfeld, and P. K. Hansma, J. Appl. Phys. **43**, 387 (1983).
- ⁷⁶J. Moreland and P. K. Hansma, Rev. Sci. Instrum. **55**, 399 (1984).
- ⁷⁷P. K. Hansma, IBM J. Res. Develop. **30**, 370 (1986).
- ⁷⁸C. T. Rogers and R. A. Buhrman, Phys. Rev. Lett. **55**, 859 (1985).
- ⁷⁹R. H. Koch, R. J. Hamers, and M. E. Welland, Bull. Am. Phys. Soc. **31**, 226 (1986).
- ⁸⁰M. Celasco, A. Masoero, P. Mazzetti, and A. Stepanescu, Phys. Rev. B **17**, 2553 (1978).
- ⁸¹R. M. Kroeker and P. K. Hansma, Surf. Sci. **67**, 362 (1977).
- ⁸²The largest peak heights that we have ever observed were for transcinnamic acid and sorbic acid, both of which have alternating double and single bonds. Spectra for these molecules are in Ref. 83.
- ⁸³J. T. Hall and P. K. Hansma, Surf. Sci. **76**, 61 (1978).
- ⁸⁴Sang-II Park and C. F. Quate, Appl. Phys. Lett. **48**, 112 (1986).
- ⁸⁵K. R. Castleman, in *Digital Image Processing* (Prentice-Hall, Englewood Cliffs, NJ, 1979), p. 201.
- ⁸⁶R. Sonnenfeld (private communication).
- ⁸⁷From Kepro Circuit Systems, Inc., via the Physics Electronics Shop, which uses it to plate printed circuit boards.
- ⁸⁸M. Howells, J. Kirz, D. Sayre, and G. Schmahl, Phys. Today **38**, 22 (August 1985).
- ⁸⁹R. V. Coleman, B. Drake, P. K. Hansma, and G. Slough, Phys. Rev. Lett. **55**, 394 (1985).
- ⁹⁰C. G. Slough, W. W. McNairy, R. V. Coleman, B. Drake, and P. K. Hansma, Phys. Rev. B **34**, 994 (1986).
- ⁹¹A. M. Baró, G. Binnig, H. Rohrer, Ch. Gerber, E. Stoll, A. Baratoff, and F. Salvan, Phys. Rev. Lett. **52**, 1304 (1984).
- ⁹²R. G. Smeenk, R. M. Tromp, J. F. van der Veen, and F. W. Saris, Surf. Sci. **95**, 156 (1980).
- ⁹³J. A. Van den Berg, L. K. Verheij, and D. G. Armour, Surf. Sci. **91**, 218 (1980).
- ⁹⁴G. Binnig, Bull. Am. Phys. Soc. **31**, 217 (1986).
- ⁹⁵A. M. Baró, R. Miranda, J. Alaman, N. Garcia, G. Binnig, H. Rohrer, Ch. Gerber, and J. L. Carrascosa, Nature **315**, 253 (1985).
- ⁹⁶J. Rabe, Ch. Gerber, J. D. Swalen, D. P. E. Smith, A. Bryant, and C. F. Quate, Bull. Am. Phys. Soc. **31**, 289 (1986).
- ⁹⁷D. W. Abraham, H. J. Mamin, E. Ganz, and J. Clarke, IBM J. Res. Develop. **30**, 492 (1986).
- ⁹⁸M. Ringger, H. R. Hidber, R. Schlögl, P. Oelhafen, and H. J. Güntherodt, Appl. Phys. Lett. **46**, 832 (1985).
- ⁹⁹M. A. McCord and R. F. W. Pease (preprint).
- ¹⁰⁰K. J. Polasko and R. F. W. Pease, Proc. SPIE **393**, 27 (1983).
- ¹⁰¹A. Muray, M. Isaacson, and I. Adesida, Appl. Phys. Lett. **45**, 589 (1984).
- ¹⁰²VG Instruments is in the process of developing a UHV tunneling microscope based on IBM Zürich designs for the heart of the microscope and a VG designed entry and sample preparation system. Leitz is studying the feasibility of manufacturing STMs for non-UHV work.
- ¹⁰³R. P. Feynman, in *Miniatrization*, edited by H. D. Gilbert (Reinhold, New York, 1961), pp. 282–296.
- ¹⁰⁴R. P. Feynman, Opt. News, 11 (February 1985).
- ¹⁰⁵C. Schneiker, *Nanotechnology*, monograph available from the author at Optical Sciences Center, University of Arizona, Tucson, AZ 85721 [(602) 621-4603]. An expanded version will appear in Harmoroff, Schneiker, and Watt, *Ultimate Computing* (Elsevier, North-Holland, Amsterdam, publication scheduled for 1987).
- ¹⁰⁶R. Gomer, IBM J. Res. Develop. **30**, 428 (1986).
- ¹⁰⁷G. Binnig, C. F. Quate, and Ch. Gerber, Phys. Rev. Lett. **56**, 930 (1986).
- ¹⁰⁸P. Murali and D. W. Pohl, Appl. Phys. Lett. **48**, 515 (1986).
- ¹⁰⁹R. M. Baum, Chem. Eng. News **64**, 22 (April 21, 1986).
- ¹¹⁰J. A. Golovchenko, Science **232**, 48 (1986).
- ¹¹¹A. L. Robinson, Science **229**, 1074 (1985).
- ¹¹²A. L. Robinson, Science **220**, 43 (1983).
- ¹¹³G. Binnig and H. Rohrer, Ultramicrosc. **11**, 157 (1983).
- ¹¹⁴G. Binnig and H. Rohrer, Surf. Sci. **152/153**, 17 (1985).
- ¹¹⁵S. Timoshenko, D. H. Young, and W. Weaver, Jr., *Vibration Problems in Engineering*, 4th ed. (Wiley, New York, 1974).
- ¹¹⁶The *Application Selection Guide*, a catalog with a clear section on design concepts, is available from Barry Controls, Watertown, MA.